A Method for Estimating the Potential Power Available to Building Mounted Wind Turbines within Turbulent Urban Air Flows

F. C. Emejeamara, A.S. Tomlin*

Low Carbon Energy Research Group, SCAPE, University of Leeds, Leeds, LS2 9JT, UK

Abstract

Small-scale wind energy applications have shown great promise in terms of their potential contribution to transitions to low carbon economies. However, the energy generation potential of such turbines within built environments has not yet been fully utilised due to the complexity of turbulent urban winds, and the challenges this creates in developing effective scoping tools for viability assessments. Effective scoping tools for turbine systems across sites within built environments require an estimation of power generated by the turbine under turbulent conditions, in addition to more commonly applied assessments based on mean wind speeds. A new methodology is therefore presented here for predicting the power generated by a turbine system operating within an urban wind resource. It was developed by employing high temporal resolution wind measurements from eight potential turbine sites within urban/suburban environments as inputs to a vertical axis wind turbine 2-D double multiple streamtube model. A relationship between turbulence intensity and the unsteady performance coefficient obtained from the turbine model was demonstrated. Hence, an analytical methodology for estimating the unsteady power coefficient at a potential turbine site is proposed. This analytical methodology was combined with an excess energy estimation model to develop a turbine power estimation (TPE) model which is used in predicting the turbine power within urban canopies. Finally, the effect of turbine control response times on the unsteady power coefficient and the turbine power estimation model was assessed. Estimates of turbine performance based on the present methodology allow a more comprehensive assessment of potential urban wind projects.

Keywords: Small-scale wind turbines; Wind power; Urban wind energy; Turbulence intensity; Excess energy content

1.0 Introduction

As global energy demands continue to grow, especially in urban areas, renewable energy sources such as solar, wind, etc., must be encouraged to share this energy burden [1, 2]. With the global energy demand in 2010 being expected to increase by 30% by 2040 [3], small wind systems are expected to serve as vital Renewable Energy Sources (RES) that are likely to represent significant portion of the energy generation mix in many power systems around the world [4, 5]. The wind resource within a built environment is characterised by highly turbulent, fluctuating winds due to enhanced local roughness, thus making it challenging to extract wind energy within such environments [6]. Siting of urban wind systems requires detailed planning and design to be able to take maximum advantage of the urban wind within a built environment. Various studies have highlighted the improvements in wind turbine output in the last 2-3 decades [7, 8]. Hence, advances in structural dynamics, aerodynamics, micrometeorology, noise level, etc., have encouraged the integration of wind systems within urban architectural designs and planning, thus suggesting the important role small wind systems will likely play in the holistic and comprehensive design of smart-city energy mix models [3, 9-11]. There are several economic and environmental benefits that arise from the integration of micro-wind systems within a suburban/urban area. To achieve this, an effective scoping tool is required to efficiently harness the available additional energy within turbulent winds, thereby reducing generation load and transmission infrastructure as well as the impact of factors such as variability, unpredictability and complexities of urban wind resource on power generation within the built environment [4, 5].

Although wind energy applications within built environments have displayed some distinct benefits, they are faced with many challenges. The complicated nature of the urban wind resource and the inability to accurately predict the potential energy generation within a built environment may lead to reduced markets as well as yields from small-scale wind technologies installed within suburban/urban areas. However, more accurate estimations of the potential annual energy generated by small-scale wind technologies may improve confidence within the market, potentially increasing wind power penetration into the electricity grid and assisting in electricity trading [12]. Increased integration of wind energy into the power grid may lead to significant social, environmental, technical and economic impacts.

Several studies have indicated that turbine systems operating within urban environments are subject to high levels of turbulence, and thus can underperform when compared to comparable turbine systems operating in less turbulent environments [13, 14]. Due to the high cost of field testing and data collection, a common approach to assessing the potential for power generation from wind turbines at a particular site is the use of power curves that have been obtained under controlled conditions, which may not perfectly reflect the conditions at the proposed site [12-19]. As a result of several investigations, it is broadly acknowledged that the power curve of a given wind turbine system is influenced by several meteorological and topographical factors like wind shear, turbulence and inclined airflow, etc. [20, 21]. Notable discrepancies are often observed between small-scale wind turbine performances predicted using manufacturer's power curves and those obtained through site specific measurements [22, 23]. A major shortcoming in most wind power assessment studies is that the wind measurements used in the development of these power curves may not fully represent the complex, fluctuating urban wind resource thus making most power curves site dependent [24]. Hence, uncertainties may arise from assumptions based on local atmospheric conditions while developing these turbine power curves. These uncertainties may lead to under or over-prediction of the turbine power output should generic power curves be applied within built environments. This, in turn, may have significant implications on the viability of urban wind projects and the wind turbine market at large.

The turbine system's ability to respond to high fluctuations present within the urban wind will be subject to the response characteristics of the specific system. A few recent studies, including those of McIntosh *et al* [25], Kooiman and Tullis [26] and Nguyen and Metzger [27], have highlighted the importance of turbine response time and its influence on energy capture within a built environment. However, to date there are no general methodologies that allow for the influence of turbulence characteristics and turbine response times on power production to be taken into account for sites across suburban/urban areas. The present work therefore attempts to fill this gap by proposing a methodology for estimating the power capabilities of small-scale wind turbine systems within a built-up area while considering the influence of local turbulence and turbine response time. A new turbine performance parameter (the turbulence induced performance coefficient) will be developed which aims to assess the performance of a turbine system while taking into account the effects of turbulence and the excess energy available at short time-scales for a potential turbine site. Field data from eight suburban/urban sites with differing characteristics will be used to develop an analytical model for predicting turbulence induced performance across different levels of turbulence intensity using a double multiple streamtube model. The influence of turbine response time on power production will then be investigated.

The paper is structured as follows. Section 2 briefly introduces the wind data employed. A brief description of the excess energy estimation model as well as a simple description of the 2-D double multiple streamtube model employed within this study are also presented in Section 2. A new model known as the turbine power estimation model (TPE), which comprises the excess energy coefficient (EEC) model and the unsteady turbine performance coefficient, is presented in Section 3.1. This model takes into account local turbulence effects and the excess energy available through turbine controls in response to turbulent fluctuations within a given suburban/urban environment. Section 3.2 considers the effect of response time on the unsteady turbine performance coefficient and turbine power estimation model. Finally, the main conclusions are presented in Section 4.

2.0 Methodology and Data Processing

2.1 Site description and Instrumentation

Based on the availability of suitable urban data sets as discussed in Ref [28], eight high-resolution wind datasets acquired from five different cities namely Leeds, Manchester, London, Dublin and Helsinki were employed in this work. Brief descriptions of these wind measurement sites are provided in Table 1 below. Detailed description of the sites are published in Ref [28].

2.2 Scope of data collected and analysis

The urban/suburban wind data employed within this study were obtained from eight sites described earlier between the years 2008 and 2011, with a year-long dataset for each site selected for analysis in this paper. For the purpose of the current analysis, these urban/suburban sites are considered as potential turbine sites based on evaluation of their mean wind speeds. Due to the unavailability of data across the chosen period (2008-2011), the datasets selected are not entirely overlapping but this does not compromise the analysis carried out in this paper. The horizontal wind components, u_{ux} (*x*-direction) and v_{uy} (*y*-direction) were used in calculating the longitudinal free-stream wind speed (V_u) and wind direction upstream of the rotor (θ_u) and are given as [28]:

$$\theta_u = \tan^{-1}(v_{uy}/u_{ux}) \quad (1)$$

$$V_u = u_{ux}\cos\theta_u + v_{uy}\sin\theta_u \quad (2)$$

while the standard deviation of the longitudinal wind speed can be calculated using Equation 3.

$$\sigma = \sqrt{\frac{1}{T}\sum_{\mathrm{i}=1}^{T}(V_{\mathrm{ui}} - \bar{V})^2} \quad (3)$$

where V_{ui} represents the free-stream wind speed upstream, $\bar{V}$ is the mean wind speed, and T characterizes the sample time period.

The high resolution wind data, obtained from all sites selected in this paper, was averaged at a sample frequency of 1 Hz to ensure data consistency between different sites, and to eliminate very fast transients. In accordance with the wind energy industry certification standards, the high resolution wind data was then parsed into contiguous 10-min bursts (i.e. T = 10 min) [34]. A standard parameter known as turbulence intensity ($T.I.$) is employed in this study. The $T.I.$ parameter in this analysis is used in characterising the degree of turbulence within a burst, and is defined in Equation 4 as follows [35]:

$$T.I.(\%) = \frac{\sigma}{\bar{V}} \times 100\% \qquad (4)$$

As represented in Equation 4, the standard deviation of the fluctuating component of the wind speed provides a measure of the degree to which the magnitude of the wind is changing during a given burst period. The $T.I.$ values for all observation sites presented within this study were calculated using Equation 4. As a result of $T.I.$ sensitivity to averaging time, turbulence intensities obtained within this study were compared for equivalent burst durations [36]. However, there exists extra energy within shorter frequencies in these high fluctuating complex urban wind conditions which is usually under-reported due to the use of mean wind speeds in calculating the wind power over a given period. This can be defined by two parameters known as the Gust Energy Coefficient (GEC) and the Excess Energy Content (EEC) [28, 36]. The GEC is defined as the ratio of the total integral kinetic energy in the wind over a given period of time to the assumed energy by only considering the mean of the wind speed within the same period [37]:

$$GEC = \frac{\int_0^T {V_i}^3 \, \mathrm{d}t}{\bar{V}^3 . T} \qquad (5)$$

where T represents the burst period.

The extra energy contained within transient fluctuation about the mean over a given burst period is represented in this paper as EEC (which is closely related to the GEC) and is expressed as a percentage of the total integral energy:

$$EEC(\%) = (GEC - 1) \times 100\% \qquad (6)$$

The values of EEC will be sensitive to the length of the burst period chosen which in this study is T = 10 min. From herein, for simplicity we drop the overbar when discussing mean wind speeds.

The average power available in the wind is calculated using Equation 7:

$$P_w = ½\rho A V^3 \qquad (7)$$

where ρ is the density of air and A is the swept rotor area.

2.4 Excess Energy Prediction Methodology

In order to estimate the excess energy content (EEC) at a given hub height within a built environment, the EEC prediction model proposed by Emejeamara and Tomlin [28] was employed. This analytical model was developed by comparing and analysing the EEC and $T.I.$ values calculated using high resolution wind measurements from potential suburban/urban turbine sites. Hence, the study suggested that the excess energy at a given hub height within a built environment at different turbulence intensities can be estimated using an empirical relationship given as:

$$EEC = 4.2B^4 + 14B^3 + 45B^2 + 99B + 74 \quad (8)$$

where

$B = (T.I. - 47)/28$.

Hence, the EEC prediction methodology, as defined in Equation 8, was adopted within this study. Further details on the EEC prediction model can be found in Refs [28, 36].

2.5 Wind Turbine Model

Various numerical models have been developed to predict and analyse the power performance of a vertical axis wind turbine system (VAWT) [38-41]. Advanced computational fluid dynamics (CFD) approaches have been used in several wind turbine studies to overcome the limitations of accuracy in aerodynamic databases for low Reynolds numbers. CFD models have the ability to calculate the turbine's aerodynamic components by integration of the Navier-Stokes equations in the neighbourhood of the wind turbine blade profile [42]. However, these CFD models have been found to be very expensive and unable to fully capture a realistic basic structure of the flow field around the blades and inside the rotor volume of the turbine when considering the selection of the meshing accuracy, physical models and the turbulence models [43]. This type of CFD approach is therefore still an area of development rather than providing a well-established, efficient and reliable technique. Since the aim of this study is to develop a scoping model for complex terrains (i.e. built environments across large cities), an analytical computationally efficient approach is required. Thus, this study employs a 2D double multiple straight-bladed VAWT streamtube model, and Blade Element Momentum (BEM) theory as the foundation for the performance model of the wind turbine system. For this analysis, three points (i.e. the free-stream region, the blade region and the wake region) as illustrated in Figure 2 will be considered.

The mass flow rate remains the same throughout the streamtube and hence the continuity equation along the streamtube can be given as:

$$\rho A V_1 = \rho A V_T = \rho A V_2 \qquad (9)$$

For steady state flow the mass flow rate across the rotor can be calculated using Equation 10:

$$\dot{m} = \rho A V_T \qquad (10)$$

Given that the mass flow rate must be the same across the streamtube, the upstream cross-sectional area of the streamtube enclosing the disc becomes smaller than the downstream cross-sectional area. Hence, the turbine experiences a thrust equal to the change in the wind's linear momentum. This is expressed by applying conservation of linear momentum on both sides of the actuator disc rotor (as expressed in Equation 11):

$$F_T = \dot{m}(V_1 - V_2) \qquad (11)$$

where V_1 and V_2 are the wind velocities upstream and downstream and $\dot{m}$ is the mass flow rate of air across the turbine rotor.

Since the flow is assumed to be frictionless and there is no work or energy transfer done, Bernoulli's equation can be applied on both sides of the rotor. Thus, applying energy conservation using the Bernoulli equation on both sides of the rotor will result in Equations 12 and 13:

$$P_{R2} + \tfrac{1}{2}\rho A V_T^2 = P_2 + \tfrac{1}{2}\rho A V_2^2 \qquad (12)$$

$$P_1 + \tfrac{1}{2}\rho A V_1^2 = P_{R1} + \tfrac{1}{2}\rho A V_T^2 \qquad (13)$$

where P_{R1} and P_{R2} are the pressures at both sides of the actuator disc as shown in Figure 2.

Combining Equations 12 and 13 gives the pressure decrease as:

$$\Delta P = \tfrac{1}{2}\rho(V_1^2 - V_2^2) \qquad (14)$$

The thrust acting on the actuator disc rotor can be calculated as the sum of the forces on each side of the rotor:

$$F_T = A\Delta P \qquad (15)$$

where

$$\Delta P = P_{R1} - P_{R2} \quad (16)$$

Thus, substituting Equation 14 into Equation 15, we have

$$F_T = ½\rho A(V_1^2 - V_2^2) \quad (17)$$

The rate at which the force (F_T) does work is expressed as $F_T V_T$, where V_T is the wind velocity across the wind turbine (which is represented as an actuator disc) and can be expressed by combining Equations 10, 11 and 17. Thus, the wind velocity across the rotor is given as:

$$V_T = \frac{V_1 + V_2}{2} \quad (18)$$

We could however, express the wind velocity downstream relative to the wind velocity upstream, giving the fractional decrease in wind speed across the wind turbine in terms of a reference factor known as the induction factor 'a'. This is expressed as:

$$a = \frac{V_1 - V_T}{V_1} = \frac{V_1 - V_2}{2V_1} \quad (19)$$

Hence from Equation 19, the wind velocity at the actuator disc V_T and the wind velocity downstream V_2 can be expressed as:

$$V_T = (1 - a)V_1 \quad (20)$$

$$V_2 = (1 - 2a)V_1 \quad (21)$$

Momentum theory applies up to $a = 0.5$, with V_2 becoming negative at higher values of a, which is obviously impossible [35, 44]. Therefore, the force of the actuator disc on flow as a result of the pressure drop introduced by the actuator disc (i.e. thrust force) can be expressed as [44]:

$$F_T = (V_1 - V_2)\rho A V_1(1 - a) \quad (22)$$

where A is the turbine rotor swept area and ρ is the air density.

Combining Equations 20, 21 and 22, the thrust force can be re-written as:

$$F_T = 2\rho A V_1^2 a(1 - a) \quad (23)$$

Thus, the thrust coefficient can also be obtained using:

$$C_T = \frac{2\rho A V_1^2 a(1-a)}{½\rho A V_1^2} = 4a(1-a) \quad (24)$$

The power extracted by the wind turbine is now given as:

$$P_T = F_T V_T = 2\rho A V_1^3 a(1-a)^2 \quad (25)$$

The performance of a turbine design can be judged using a coefficient known as the turbine power coefficient (C_p). This is basically defined as the percentage of wind power the turbine can convert to mechanical power and is mathematically represented by:

$$C_p = \frac{P_T}{P_w} \quad (26)$$

where P_T is the power captured by the turbine, P_w is the power available in the wind for the size of turbine.

Substituting Equations 7 and 25 into Equation 26**,** the power coefficient can then be expressed as:

$$C_p = \frac{2\rho A V_1^3 a(1-a)^2}{½\rho A V_1^3} = 4a(1-a)^2 \quad (27)$$

Thus, while assuming the control volume boundaries are the surface of a streamtube (as shown in Figure 2), the BEM theory basically utilises the actuator disc method which is based on a control volume analysis to calculate the momentum deficit downstream [27, 35, 45]. This is combined with empirical lift and drag coefficients of the turbine blades (airfoil sections) in order to calculate the power performance of the turbine employed in this study [25, 39].

Although straight-bladed Darrieus type vertical axis wind turbine (VAWT) is known as the simplest wind turbine, its aerodynamic analysis is quite complex. The dynamic stall VAWT turbine modelling work within this study is based on the previous works of McIntosh *et al* [25], Beri and Yao [45] and Homicz [46]. In order to accomplish this, the turbine is divided into multiple strips and the lift and drag forces at the corresponding angle of attack acting on the turbine blades can be calculated using the empirical lift and drag coefficient data appropriate for the blade (airfoil) type or section. This is achieved by using a look-up table containing the lift and drag coefficients (C_l and C_d respectively) as a function of the local Reynolds number (Re) and the angle of attack (α). Figure A.1 presents a simple description of the forces (i.e. the lift and drag forces) acting on the turbine blade (See Appendix 1). From Figure 3, the angle of attack is shown to be dependent on the relative velocity (V_r).

Thus,

$$\alpha = \tan^{-1}\left(\frac{V_n}{V_t}\right) = \tan^{-1}\left(\frac{(1-a)sin\theta}{(1-a)cos\theta + \lambda}\right) \quad (28)$$

where θ is the blade azimuthal angle, V_n and V_t are the normal and tangential velocity components and λ represents tip speed ratio (which is defined as $\frac{\omega R}{V_\infty}$, where ω represents the rotational speed of the rotor and R is the rotor radius).

The normal and tangential forces acting on the turbine blades can be calculated using Equations 29 and 30:

$$F_n = \frac{1}{2}\rho ncH(C_l cos\alpha + C_d sin\alpha)\, {V_r}^2 \quad (29)$$

$$F_t = \frac{1}{2}\rho ncH(C_l sin\alpha - C_d cos\alpha)\, {V_r}^2 \quad (30)$$

where c represents the chordlength of the blade, C_l represents the lift coefficient, C_d represents the drag coefficient, H denotes the blade height and n is the number of turbine blades.

The average torque on the turbine rotor in a full revolution can be estimated using Equation 31:

$$T_{ba} = N\sum_{i=1}^{2m}\frac{\left[\frac{1}{2}\rho HcRV_r^2C_t\right]}{2m} \quad (31)$$

where m is the number of stream tubes and $2m$ is the number of $\Delta\theta$.

The torque and power coefficients can then be derived from Equations 32 and 33:

$$C_q = \frac{T_{ba}}{\frac{1}{2}\rho DRH{V_\infty}^2} \quad (32)$$

and the power coefficient can be rewritten as:

$$C_p = C_q.\lambda \quad (33)$$

For this study, a NACA airfoil with a chordlength of 0.08815 m and a turbine rotor diameter and blade height of 1.5 m was considered. This study includes the dynamic stall model presented by Ref [48] with corrections from Refs [39,40]. As shown by other BEM models [25, 27, 35, 39, 45, 46], the VAWT model uses a database of static NACA00** airfoil lift and drag coefficients obtained from wind tunnel tests by Sheldahl and Klimas [49] and later corrected by Lazauskas [50]. Thus, the C_l and C_d are interpolated for the relevant Reynolds number and angle of attack. This model however does not consider wind shear, electrical, aerodynamic and tower losses. As shown in Figure 4, the

VAWT model performance showed good agreement with predicted power coefficients over a range of tip speed ratios for data obtained for a VAWT numerical model presented by McIntosh *et al* [25].

For the purposes of this study, a 600 W variable speed control (VSC) VAWT system was considered, thus representing a micro-wind turbine system for domestic electricity generation [51]. The turbine system considered is assumed to be a three straight-bladed NACA0015 VAWT. This study also employs an ideal tip speed ratio controller, which allows the turbine system to respond instantaneously to fluctuations in the wind, thereby extracting the maximum amount of energy available from the wind. Thus, the controller adjusts the ω while responding to the fluctuations in the incoming wind in order to ensure that the turbine operates within the optimal C_p-λ setting. In practice, power electronics are used in variable speed control operations. Although more advanced controls can be found in commercial wind turbine systems, a simple feedback control is used within this study. In reality, the response time for a wind turbine system depends on the mass moment of inertia of the turbine as well as the gain constant of the controller [25, 27, 44]. With real-time wind data as inputs, the time varying rotational speed, tip speed ratio, aerodynamic torque and power were determined as a function of time from the BEM model described above. Within practical systems, additional losses such as electrical, aerodynamic and tower losses will be experienced [35, 52, 53]. Such additional losses have not been directly addressed within the current work which is focussed around the influence of turbulent wind profiles. Further modifications to the power coefficient due to such losses for specific turbine designs could be added within the practical application of such a model but this extends beyond the scope of the present work**.** Figure 5 demonstrates the performance of the VAWT numerical model as described above.

3.0 Results and Discussion

3.1 Turbine Power Estimation Model

Generally, power generated by a turbine can be rewritten as [15]:

$$P_T = \frac{1}{2} C_p \rho A V^3 \qquad (34)$$

where C_p represents the power coefficient of the turbine system, ρ represents the air density, A represents the rotor swept area and V is the mean wind speed over a burst period. Various studies have adopted Equation 34 in their power assessment studies and also demonstrated the effect of turbulence on turbine power by adopting measures of factoring turbulence intensity into turbine power estimation. This has been achieved either by directly using $T.I.$ as a form of heuristic safety factor (i.e. reducing the turbine power estimation by its percentage value [51]) or by adjusting or correcting the manufacturer's power curve for different turbulence intensity values [13]. These require complex methodologies which may not be user-friendly or readily accessible to micro-turbine purchasers or investors. It should be noted that turbine manufacturers are currently not required (by an industry standard or practice) to rate their turbine systems for an arbitrary or more realistic turbulence intensity. As turbulence levels within an urban wind resource increase or decrease, the C_p (as represented in Equation 34) has to be adjusted to account for inherent local turbulence. In order to estimate the power generated by the VAWT within a characteristic urban wind resource, a methodology is proposed herein. This methodology, which estimates the turbine power from averaged wind over a built environment within a given burst period, is referred to as the turbine power estimation (*TPE*) model and is mathematically given as:

$$TPE = P_{T\_pred} = \frac{1}{2} C_{tc} \rho A \bar{V}^3 \qquad (35)$$

Similar to Equation 34, C_p is replaced by a new parameter C_{tc} in Equation 35, which is termed the turbulence induced performance coefficient of the turbine system. C_{tc} is mathematically given as:

$$C_{tc} = C_e(EEC + 1) \qquad (36)$$

where EEC is the excess energy content at a given burst period within the potential turbine site (defined by Equation 8) and C_e is the unsteady turbine performance coefficient.

The performance coefficient C_{tc} takes into account the effect of turbulence and response time on the turbine performance while also considering the excess energy content available to the turbine. In order to predict the C_e for a given VAWT system within a built environment, the C_e for a given burst period of 10 min (i.e. T = 10 min) across the year was obtained using Equation 37 and plotted against the equivalent binned values of $T.I.$ for the 8 test sites.

$$C_e = \frac{\int_0^T P_{vsc}\, dt}{\int_0^T P_w\, dt} \qquad (37)$$

where P_{vsc} represents the instantaneous VAWT power outputs from model simulations using the turbine system model (as presented in Section 2.5) at response time of 1 s using the wind datasets from the eight sites as inputs, and P_w represents the instantaneous wind power calculated using Equation 38:

$$P_w = \frac{1}{2}\rho A V_i^3 \tag{38}$$

where V_i represents the wind speed measurements at a given averaging time (in this case, T_c = 1 s). The wind speed measurements were obtained as described in Section 2.2.

For an ideal (i.e. perfect) turbine operation within an idealised steady wind environment, the C_{tc} would be 0.59 (i.e. C_e and EEC would be 0.59 (the Betz limit for HAWT whereas that for VAWT is somewhat lower primarily due to a drag-based, as opposed to a lift-based, operating system [35, 38, 54]) and 0 respectively). This indicates that the excess energy and turbine performance calculated, reflects the time-series integral. However, due to real world gustiness and losses encountered by the turbine system while operating at potential sites (for example, transmission losses, electrical losses, etc.), this may not be realised. When analysing the unsteady turbine performance, the turbine response was first assumed to be 1 s and the raw wind data was also filtered at an averaging time (T_c) of 1 s, as stated earlier. Losses encountered in turbine operations (i.e. electrical losses, strut losses, mechanical losses, etc.) were not considered herein and hence the estimations are likely to be the upper limit compared to what might be realised in practice. Plots of binned C_e values against $T.I.$ bins as shown in Figure 6 demonstrate a strong relationship between C_e and $T.I.$ with increases in $T.I.$ resulting in decreased turbine performance at all test sites. An empirical equation for the prediction of C_e values as a function of $T.I.$ was determined using the least square errors approach within MATLAB's best fit tool. After various tests to determine the lowest errors, a single-term exponential form was assumed, hence C_e values were approximated using the following empirical relationship:

$$C_e = ae^{cx} \tag{39}$$

where

$x = (T.I. - q)/s$

Table 1 presents the coefficients derived from best fit of a $C_e - T.I.$ curve at a response time of 1 s (i.e. T_c = 1) shown in Figure 6. This suggests that from the knowledge of turbulence intensities, the performance of a given turbine design could be estimated. However, further analysis showed that increasing the turbine inertia may lead to a decrease in the power generated by the turbine system. This is demonstrated in Figure 7, by comparing the performance of the turbine system having a standard baseline inertia (*J*) with the turbine performance when the standard baseline inertia is increased by 20% (represented by '$J + 20\% J$' in Figure 7). Results show a significant decrease of approximately 24.4% in turbine performance observed at the Leeds (H1) site should the turbine system experience a 20% increase in its inertia. Hence, from Equations 35 and 36, one can deduce a decrease of 24.4% in the power predicted using the *TPE* model should the turbine inertia be increased by 20%. This, however, suggests that the turbine inertia has a big impact on the power generated by turbine system, as well as the overall economic benefits for potential urban wind projects. Thus, further sensitivity analysis testing the effects of inertia on the turbine power estimation (*TPE*) model would be useful in future work.

EEC values were calculated using the EEC model as proposed in Section 2.4. Thus, incorporating Equation 8 and Equation 39 into Equations 36, the turbine power output at a potential site which takes into account the effect of local turbulence can be estimated using Equation 35. A comparison of errors between the turbine power estimation model values (P_{T_pred}) and power output obtained from VSC VAWT model simulations (P_{VSC}) at a burst period of 10 mins using wind data from all 8 sites as input was achieved by using the mean percentage error (MPE) as defined in Equation 40. Figure 8 presents the MPE at different $T.I.$ bins for all 8 sites.

$$\text{MPE}(\%) = 100 \times \frac{1}{n} \sum \frac{|P_{VSC} - P_{T\_pred}|}{P_{VSC}} \qquad (40)$$

As demonstrated in Figure 8, *TPE* model errors for $T.I.$ between 40 – 60% were shown to be as low as 15.7%. A wide range of turbulence intensities were seen in the experimental data. Whilst it may not be common for sites to experience high levels of T.I. > 50% these values are possible and were demonstrated in Figure 6 to occur within several cities. They are likely to occur under low mean wind speed conditions, when local sources of turbulence such as building induced eddies, buoyancy effects and possibly even traffic induced turbulence may dominate over mean wind effects. Their low frequency of occurrence presents a challenge for the model and further analysis showed higher *TPE* model errors within Dublin Marrowbone and Helsinki Suburban sites. This may have resulted from a lower occurrence of data within this $T.I.$ bin (See Appendix 2), thus suggesting reduced level of model accuracy of the *TPE* model within 40-60% $T.I.$ bins. Also, *TPE* model errors within the 20 – 30% $T.I.$ bin were observed to be low across all sites except the London site where the occurrence of such conditions were less frequent (See Appendix 2). Hence, the *TPE* model showed fairly good performance at all sites for turbulence intensities between 20 – 60%, which represented the dominant $T.I.$ demonstrated by the $T.I.$ frequency distribution (as shown in Figure 8). Turbine power predictions at $T.I.$ less than 20% and also within the 60 – 70% bin resulted in errors as high as 25.6%. A poor performance was also observed at $T.I.$ higher than 70% across all sites. This was expected at these turbulence intensities as the occurrence of such turbulent conditions will be less frequent within built environments (as demonstrated in Figure 8 and Appendix 2). As shown in Figure 9, the average power output estimation using *TPE* model is found to have a positive correlation with VAWT power outputs thus implying better turbine power estimation. It will be interesting to compare average power outputs from turbines using advanced controls and the *TPE* model. Hence, these results suggest the possibility of predicting turbine power fairly well by using a simple model within a built environment as long as the local mean wind speed and $T.I.$ are known.

3.2 Effect of T_c on C_e and Turbine Power Estimation

Turbine response time has been shown to significantly influence the energy capture within an urban wind resource [27]. Considering the influence of various factors such as turbine inertia, higher local gust frequencies, time lag experienced by controllers, etc., on turbine operations, turbine systems with a response time of 1 s may not be feasible in real world applications within built environments. Hence, different response times were considered to assess the effect on turbine power output within an urban wind resource for potentially different VAWT designs. This is demonstrated by calculating the unsteady turbine performance coefficient (C_e) at different response times of 10 s, 20 s and 30 s within a burst period of 10 min using Equation 37. These C_e values plotted against the equivalent binned values of $T.I.$ at the eight potential turbine sites are presented in Figure 10. The best fit for C_e - $T.I.$ plots at different response times were determined using the least square errors approach within MATLAB's best fit tool. After various tests to determine the lowest errors, a two-term exponential form was assumed for response times of 10 s, 20 s and 30 s. Hence, C_e values were approximated using the following empirical relationship:

$$C_e = ae^{cx} + be^{dx} \qquad (41)$$

where

$$x = (T.I. - q)/s$$

A summary of the coefficients of the two-term exponential for the different response times are provided in Table 2. The maximum response time considered within this study was 30 s above which the turbine system may be considered uneconomical for operations within a built environment.

As shown in Figure 10, it was observed that as the response time of the turbine increased, the C_e - $T.I.$ curve was observed to be steeper at lower turbulence intensities (represented by the first term of the exponential in Equation 41) and flatter at higher turbulence intensities (represented by the second term of the exponential). A simple plot distinguishing the first and second terms of the exponential in Equation 41 is demonstrated in Figure 10d. Thus, Figure 10 suggests that as the response time approaches 30 s, less significant changes in the turbine's power output may be observed at higher turbulence intensities, whereas a steep increase in power may be observed at lower turbulence intensities as the turbine becomes less sensitive to wind fluctuations. These relationships obtained at different response times (as represented by the coefficients in Table 2) were employed in calculating the turbulence induced power coefficient (C_{tc}) using Equation 36. Thus, they served as inputs in estimating turbine power across the 8 potential sites using Equation 35.

The VAWT model power outputs across the 8 potential sites were obtained by using wind data filtered at averaging times of 10 s, 20 s and 30 s as input to the turbine model with VSC controls. These outputs were compared with turbine power prediction model outputs using the mean percentage error (MPE) parameter defined by Equation 40. Figure 11 presents MPE plots across different $T.I.$ bins at different response times for all eight sites. Results show good *TPE* performance at a response time of 10 s, with power prediction errors less than 16% at turbulence intensities below 40%. Further analysis showed over 90% of the wind resource across the 8 test sites to have occurred at $T.I.$ below 40%. High *TPE* model errors were observed at higher turbulence intensities (i.e. $T.I.$ > 50 %) which represent a very small percentage of the wind resource at the test sites. The *TPE* model demonstrated good power predictions at the response times of 20 s and 30 s (as shown in Figure 10). However, higher errors were observed in less frequent turbulence intensity bins (i.e. $10 - 20\%$ $T.I.$ bin and at $T.I.$ > 50%). This is in agreement with results obtained at a response time of 10 s (as shown in Figure 11 a). Further analysis showed these high errors were as a result of poor model accuracy at Helsinki (suburban and urban) and Dublin Marrowbone sites due to these turbulence intensity bins being less frequent. Figure 12 presents the overall average MPE for different response times at all eight sites with average model errors of 14.11%, 14.51%, 15.64% and 13.33% at response times of 1 s, 10 s, 20 s and 30 s respectively.

4.0 Conclusions

Developing power curves used in performance assessment studies from assumptions based on local atmospheric conditions may lead to various uncertainties such as under-prediction or over-prediction of the actual power generated by urban wind applications. These uncertainties can be reduced by incorporating factors such as turbulence, inertia, and turbine response time when estimating the power generated by the turbine system. A new turbine performance parameter known as the turbulence induced performance coefficient (C_{tc}) was introduced in this paper. This parameter aims to assess the performance of a turbine system while taking into account the effect of turbulence (as represented by the unsteady performance coefficient, C_e) and excess energy available at a potential turbine site. An analytical model for predicting C_e at different turbulence intensities was developed using data collected from eight suburban/urban sites as inputs within a micro wind turbine VSC VAWT model. Hence, a methodology for estimating the turbine power output within a gusty wind resource was proposed by multiplying the C_{tc} value with the wind energy available to the turbine system for a given burst period. The effect on turbine response time on turbine performance was also presented and discussed. Hence, considering factors such as turbulence intensity and response time, results presented in this paper demonstrated the possibility of estimating power that would be generated by a turbine system thus encouraging effective assessment of the viability of urban wind projects. It would be useful in future work to test the viability of this methodology for various types of wind turbine control systems. The methodology proposed also provides the opportunity to map the potential power generated by a turbine system for different mast heights over city regions assuming the mean wind speed and turbulence intensities can be estimated. This will be addressed in future work, allowing the assessment of the viability of urban wind projects by mapping the capacity factor over built environments that takes into account the spatial variability in not just the mean winds, but also the turbulence intensities.

Acknowledgement

The authors would like to thank Leena Järvi, Curtis Wood and Annika Nordbo (The University of Helsinki), Keith Sunderland (Dublin Institute of Technology), James Gooding (University of Leeds), Joel Millward-Hopkins and all the parties involved in providing valuable data used in this study.

REFERENCES

1. Martinez Soto, A. and Jentsch, M.F. Comparison of prediction models for determining energy demand in the residential sector of a country. *Energy and Buildings.* 2016, **128**, pp.38-55.
2. Cooney, C., Byrne, R., Lyons, W. and O'Rourke, F. Performance characterisation of a commercial-scale wind turbine operating in an urban environment, using real data. *Energy for Sustainable Development.* 2017, **36**, pp.44-54.
3. Dashwood, J. Australia's Energy Options: Renewables efficiency. Chapter 4. The outlook for energy: A view to 2040. 2012, p.45.
4. Catalão, J.P. *Smart and sustainable power systems: operations, planning, and economics of insular electricity grids.* CRC Press, 2017.
5. Ishugah, T., Li, Y., Wang, R., Kiplagat, J.J.R. and reviews, s.e. Advances in wind energy resource exploitation in urban environment: A review. 2014, **37**, pp.613-626.
6. Lee, K.-Y., Tsao, S.-H., Tzeng, C.-W. and Lin, H.-J. Influence of the vertical wind and wind direction on the power output of a small vertical-axis wind turbine installed on the rooftop of a building. *Applied Energy.* 2018, **209**, pp.383-391.
7. Hameed, Z., Hong, Y., Cho, Y., Ahn, S., Song, C.J.R. and reviews, S.e. Condition monitoring and fault detection of wind turbines and related algorithms: A review. 2009, **13**(1), pp.1-39.
8. Islam, M., Mekhilef, S., Saidur, R.J.R. and Reviews, S.E. Progress and recent trends of wind energy technology. 2013, **21**, pp.456-468.
9. Grant, A., Johnstone, C. and Kelly, N.J.R.E. Urban wind energy conversion: The potential of ducted turbines. 2008, **33**(6), pp.1157-1163.
10. Calvillo, C.F., Sánchez-Miralles, A., Villar, J.J.R. and Reviews, S.E. Energy management and planning in smart cities. 2016, **55**, pp.273-287.
11. Panagiotis, K., Lambros, E. and (Eds). *Electricity Distribution, Intelligent Solutions for Electricity Transmission and Distribution Networks.* Springer-Verlag Berlin Heidelberg, 2016.

12. Lydia, M., Suresh Kumar, S., Immanuel Selvakumar, A. and Edwin Prem Kumar, G. Wind resource estimation using wind speed and power curve models. *Renewable Energy.* 2015, **83**, pp.425-434.
13. Sunderland, K., Woolmington, T., Blackledge, J. and Conlon, M. Small wind turbines in turbulent (urban) environments: A consideration of normal and Weibull distributions for power prediction. *Journal of Wind Engineering and Industrial Aerodynamics.* 2013, **121**, pp.70-81.
14. Battisti, L., Benini, E., Brighenti, A., Dell'Anna, S. and Raciti Castelli, M. Small wind turbine effectiveness in the urban environment. *Renewable Energy.* 2018, **129**, pp.102-113.
15. Acosta, J.L., Combe, K., Djokic, S.Z. and Hernando-Gil, I. Performance assessment of micro and small-scale wind turbines in urban areas. *Systems Journal, IEEE.* 2012, **6**(1), pp.152-163.
16. Kaiser, K., Langreder, W., Hohlen, H. and Hojstrup, J. Turbulence Correction of Power Curve. In: Peinke, J. et al. eds. *Wind Energy: Proceedings of the Euromech Colloquium*. New York: Springer, 2007, pp.159-162.
17. Acosta, J.L. Assessment of renewable wind resources in UK urban areas. In: *MELECON 2010-2010 15th IEEE Mediterranean Electrotechnical Conference*: IEEE, 2010, pp.1439-1444.
18. Lydia, M., Kumar, S.S., Selvakumar, A.I. and Prem Kumar, G.E. A comprehensive review on wind turbine power curve modeling techniques. *Renewable and Sustainable Energy Reviews.* 2014, **30**, pp.452-460.
19. Byrne, R., Hewitt, N.J., Griffiths, P. and MacArtain, P. Observed site obstacle impacts on the energy performance of a large scale urban wind turbine using an electrical energy rose. *Energy for Sustainable Development.* 2018, **43**, pp.23-37.
20. Wagner, R., Antoniou, I., Pedersen, S.M., Courtney, M.S. and Jørgensen, H.E. The influence of the wind speed profile on wind turbine performance measurements. *Wind Energy.* 2009, **12**(4), pp.348-362.
21. Lubitz, W.D. Impact of ambient turbulence on performance of a small wind turbine. *Renewable Energy.* 2014, **61**, pp.69-73.
22. Pagnini, L.C., Burlando, M. and Repetto, M.P. Experimental power curve of small-size wind turbines in turbulent urban environment. *Applied Energy.* 2015, **154**, pp.112-121.
23. Whale, J., McHenry, M.P. and Malla, A. Scheduling and conducting power performance testing of a small wind turbine. *Renewable Energy.* 2013, **55**, pp.55-61.
24. Trivellato, F., Battisti, L. and Miori, G. The ideal power curve of small wind turbines from field data. *Journal of Wind Engineering and Industrial Aerodynamics.* 2012, **107-108**, pp.263-273.

25. McIntosh, S., Babinsky, H. and Bertenyi, T. Optimizing the Energy Output of Vertical Axis Wind Turbines for Fluctuating Wind Conditions. In: *45th AIAA Aerospace Sciences Meeting and Exhibit*. Reno, Nevada, USA: American Institute of Aeronautics and Astronautics, 2007.

26. Kooiman, S. and Tullis, S. Response of a vertical axis wind turbine to time varying wind conditions found within the urban environment. *Wind Engineering.* 2005, **34**(4), pp.389-401.

27. Nguyen, L. and Metzger, M. Enhanced energy capture by a vertical axis wind turbine during gusty winds in an urban/suburban environment. *Journal of Renewable and Sustainable Energy.* 2015, **7**(5), p.053118.

28. Emejeamara, F. and Tomlin, A. A method for mapping the turbulence intensity and excess energy available to building mounted wind turbines over a UK City. *Wind Energy.* 2016, **19**(8), pp.1423-1438.

29. Järvi, L., Hannuniemi, H., Hussein, T., Junninen, H., Aalto, P.P., Hillamo, R., Mäkelä, T., Keronen, P., Siivola, E. and Vesala, T. The urban measurement station SMEAR III: Continuous monitoring of air pollution and surface-atmosphere interactions in Helsinki, Finland. *Boreal environment research.* 2009, **14**, pp.86-109.

30. Nordbo, A., Järvi, L., Haapanala, S., Moilanen, J. and Vesala, T. Intra-city variation in urban morphology and turbulence structure in Helsinki, Finland. *Boundary-Layer Meteorology.* 2013, **146**(3), pp.469-496.

31. Wood, C.R., Barlow, J.F., Belcher, S.E., Dobre, A., Arnold, S.J., Balogun, A.A., Lingard, J.J., Smalley, R.J., Tate, J.E. and Tomlin, A.S. Dispersion experiments in central London: the 2007 DAPPLE project. *Bulletin of the American Meteorological Society.* 2009, **90**(7), pp.955-969.

32. Barlow, J., Dobre, A., Smalley, R., Arnold, S., Tomlin, A. and Belcher, S. Referencing of street-level flows measured during the DAPPLE 2004 campaign. *Atmospheric Environment.* 2009, **43**(34), pp.5536-5544.

33. Balogun, A.A., Tomlin, A.S., Wood, C.R., Barlow, J.F., Belcher, S.E., Smalley, R.J., Lingard, J.J., Arnold, S.J., Dobre, A. and Robins, A.G. In-street wind direction variability in the vicinity of a busy intersection in central London. *Boundary-Layer Meteorology.* 2010, **136**(3), pp.489-513.

34. IEC 61400-12-1. *Wind Turbines – Part 12-1 : Power performance measurement of Electricity producing wind turbines.* 2005.

35. Burton, T., Sharpe, D., Jenkins, N. and Bossanyi, E. *Wind Energy Handbook.* John Wiley & Sons Ltd, West Sussex, UK, 2001.

36. Emejeamara, F.C., Tomlin, A.S. and Millward-Hopkins, J.T. Urban wind: Characterisation of useful gust and energy capture. *Renewable Energy.* 2015, **81**, pp.162-172.

37. Bertényi, T., Wickins, C. and McIntosh, S. Enhanced energy capture through gust-tracking in the urban wind environment. In: *48th AIAA Aerospace Sciences Meeting*, *Orlando, Florida, USA*. American Institute of Aeronautics and Astronautics, 2010.

38. Islam, M., Ting, D. and Fartaj, A. Aerodynamic Models for Darrieus-type Straight-bladed Vertical Axis Wind Turbines. *Renewable and Sustainable Energy Reviews.* 2008, **12(4)**, pp.1087-1109.

39. Paraschivoiu, I. Double-multiple streamtube model for darrieus wind turbines. 1981, **Second DOE/NASA wind turbines dynamics workshop, NASA CP-2186, Cleveland, OH**, pp.19–25.

40. Staelens, Y., Saeed, F. and Paraschivoiu, I. A Straight-Bladed Variable-Pitch VAWT Concept for Improved Power Generation. *In: 41st Aerospace sciences meeting and exhibit, Reno, NV, USA.* 2003.

41. McIntosh, S.C. *Wind energy for the built environment*. thesis, University of Cambridge, 2009.

42. Castelli, M.R., Englaro, A. and Benini, E. The Darrieus wind turbine: Proposal for a new performance prediction model based on CFD. *Energy.* 2011, **36**(8), pp.4919-4934.

43. Mohamed, M.H., Ali, A.M. and Hafiz, A.A. CFD analysis for H-rotor Darrieus turbine as a low speed wind energy converter. *Engineering Science and Technology, an International Journal.* 2015, **18**(1), pp.1-13.

44. Bianchi, F.D., De Battista, H. and Mantz, R.J. *Wind turbine control systems: principles, modelling and gain scheduling design.* Springer Science & Business Media, 2006.

45. Beri, H. and Yao, Y. Double Multiple Stream Tube Model and Numerical Analysis of Vertical Axis Wind Turbine. *Energy and Power Engineering Journal.* 2011, **3**, pp.262-270.

46. Homicz, G.F. Numerical Simulation of VAWT Stochastic Aerodynamic Loads Produced by Atmospheric Turbulence: VAWT-SAL Code. *Sandia Laboratories Energy Report.* 1991, **SAND91 - 1124**.

47. Nahas, M.N. A Self-Starting Darrieus-Type Windmill. *Energy and Power Engineering Journal.* 1993, **18**(9), pp.899 - 906.

48. Gormont, R.E. An Analytical Model of Unsteady Aerodynamics and Radial Flow for Application to Helicopter Rotors. *U.S. Army Air Mobility Research and Development Laboratory Technical Report.* 1973, **72-67**.

49. Sheldahl, R.E. and Klimas, P.C. *Aerodynamic characteristics of seven symmetrical airfoil sections through 180-degree angle of attack for use in aerodynamic analysis of vertical axis wind turbines.* Sandia National Labs., Albuquerque, NM (USA), 1981.

50. Lazauskas, L. Three pitch control systems for vertical axis wind turbines compared. *Wind Engineering.* 1992, **16**(5), pp.269-282.

51. Allen, S., Hammond, G. and McManus, M. Energy analysis and environmental life cycle assessment of a micro-wind turbine. *Proceedings of the Institution of Mechanical Engineers, Part A: Journal of Power and Energy.* 2008, **222**(7), pp.669-684.
52. Adaramola, M.S. and Krogstad, P.Å. Experimental investigation of wake effects on wind turbine performance. *Renewable Energy.* 2011, **36**(8), pp.2078-2086.
53. Heide, D., von Bremen, L., Greiner, M., Hoffmann, C., Speckmann, M. and Bofinger, S. Seasonal optimal mix of wind and solar power in a future, highly renewable Europe. *Renewable Energy.* 2010, **35**(11), pp.2483-2489.
54. Weimer, M.A., Paing, T.S. and Zane, R.A. Remote area wind energy harvesting for low-power autonomous sensors. In: *2006 37th IEEE Power Electronics Specialists Conference*: IEEE, 2006, pp.1-5.
55. Manwell, J.F., McGowan, J.G. and Rogers, A.L. *Wind Energy Explained: Theory, Design and Application.* Second ed. John Wiley & Sons Ltd, West Sussex, UK, 2002.

Table 1: Brief description of the wind measurement sites

Site Label	Site Description	Site Cordinate	Anemometer Type	Sampling Frequency	Measurement Height
Unileeds H1	Houldsworth building, University of Leeds Campus, Leeds, UK. Ref [28]	Lat.: 53.467371°, Long.: -2.232006°	Research-Grade Gill Scientific Instruments model R3-50	10 Hz	Building height approximately 24 m, mast height of 10m
Unileeds H2	Houldsworth building, University of Leeds Campus, Leeds, UK. Ref [28]	Lat.: 53.467371°, Long.: -2.232006°	Research-Grade Gill Scientific Instruments model R3-50	10 Hz	Building height approximately 24 m, mast height of 6m
Manchester	The George Kenyon building within the University of Manchester South campus (also known as the Whitworth	Lat.: 53.467371°, Long.: -2.232006°	Gill Windmaster Pro Sonic Anemometer	20Hz	Mast height approximately 5 m, building height of 49m

	Meteorological Observatory. Ref [28]				
Dublin Marrowbone	Dublin City Council Building in Marrowbone Lane. Ref [13]	Lat.: 53.337767° , Long.: -6.286186°	Campbell Scientific CSAT3 three-dimension al sonic anemometer	10 Hz	Total measurement height of approximately 17 m
Dubline St Pius X	St. Pius X National (Girls) School. Ref [13]	Lat.: 53.337767° , Long.: -60.305283°	Campbell Scientific CSAT3 three-dimension al sonic anemometer	10 Hz	Total measurement height of approximately 12 m
Helsinki Urban	Roof-top of Hotel Torni within Helsinki city. Ref [29, 30]	Lat.: 60.167803° , Long.: 24.938689°	Metek USA-1 three-dimension al ultrasonic anemometer	10 Hz	Mast height approximately 2.3 m, total building height approximately 42.7 m
Helsinki Suburban	SMEAR III (Station for Measuring Ecosystem-Atmosphere Relationships). Ref [29, 30]	Lat.: 60.202817°, Long.: 24.961128°	Metek USA-1 three-dimension al ultrasonic anemometer	10 Hz	Mast at the height of 31 m with the anemometer located on a horizontal boom
London	The Westminster city council building, London. Ref [31-33]	Lat.: 51.521588°, Long.: -0.160074°	Gill R3-100 sonic anemometer	20Hz	Mast height approximately 3.5 m, building height approximately 15 m

Table 2: Coefficients used in predicting the unsteady power coefficient required for the power estimation model (as given in Equation 39).

Constants	
a	23.85
c	-0.7476
q	43.32
s	21.32

Table 3: Summary of the coefficients for the best fit for $C_e - T.I.$ plots at different response times across the 8 sites.

Constants	**Turbine Response time (s)**		
	10	**20**	**30**
a	19.02	23.51	0.6099
b	3.789	1.045	19.84
c	-0.4299	-0.5336	-3.342
d	-1.806	-2.881	-0.2464
q	41.19	35.99	35.79
s	21.2	21.03	20.95

Appendix 3.1

			Lift	Coefficient	for NACA0012	
--------------------------------			REYNOLDS	NUMBER	-----------------------	
ALPHA	160000	360000	700000	1000000	2000000	5000000
0	0	0	0	0	0	0
1	0.11	0.11	0.11	0.11	0.11	0.11
2	0.22	0.22	0.22	0.22	0.22	0.22
3	0.33	0.33	0.33	0.33	0.33	0.33
4	0.44	0.44	0.44	0.44	0.44	0.44
5	0.55	0.55	0.55	0.55	0.55	0.55
6	0.66	0.66	0.66	0.66	0.66	0.66
7	0.746	0.77	0.77	0.77	0.77	0.77
8	0.8247	0.8542	0.88	0.88	0.88	0.88
9	0.8527	0.9352	0.9598	0.9661	0.99	0.99
10	0.1325	0.9811	1.0343	1.0512	1.0727	1.1
11	0.1095	0.9132	1.0749	1.1097	1.1539	1.1842
12	0.1533	0.4832	1.039	1.1212	1.2072	1.2673
13	0.203	0.2759	0.8737	1.0487	1.2169	1.3242
14	0.2546	0.2893	0.6284	0.8846	1.1614	1.3423
15	0.3082	0.3306	0.4907	0.7108	1.0478	1.3093
16	0.362	0.3792	0.4696	0.606	0.9221	1.2195
17	0.42	0.4455	0.5195	0.5906	0.7826	1.0365
18	0.4768	0.5047	0.5584	0.603	0.7163	0.9054
19	0.5322	0.5591	0.6032	0.6334	0.7091	0.8412
20	0.587	0.612	0.6474	0.6716	0.7269	0.8233
21	0.6414	0.6643	0.6949	0.7162	0.7595	0.8327
22	0.6956	0.7179	0.7446	0.7613	0.7981	0.8563
23	0.7497	0.7715	0.7948	0.8097	0.8429	0.8903
24	0.8043	0.8246	0.8462	0.8589	0.8882	0.9295
25	0.8572	0.878	0.8984	0.9093	0.9352	0.9718
26	0.9109	0.9313	0.9506	0.9618	0.9842	1.0193
27	0.923	0.9412	0.9583	0.9683	0.9882	1.068
30	0.9593	0.9709	0.9814	0.9878	1.002	0.915
35	1.02	1.02	1.02	1.02	1.02	1.02
40	1.075	1.075	1.075	1.075	1.075	1.075
45	1.085	1.085	1.085	1.085	1.085	1.085
50	1.04	1.04	1.04	1.04	1.04	1.04
55	0.965	0.965	0.965	0.965	0.965	0.965
60	0.875	0.875	0.875	0.875	0.875	0.875
65	0.765	0.765	0.765	0.765	0.765	0.765
70	0.65	0.65	0.65	0.65	0.65	0.65
75	0.515	0.515	0.515	0.515	0.515	0.515
80	0.37	0.37	0.37	0.37	0.37	0.37
85	0.22	0.22	0.22	0.22	0.22	0.22
90	0.07	0.07	0.07	0.07	0.07	0.07
95	-0.07	-0.07	-0.07	-0.07	-0.07	-0.07
100	-0.22	-0.22	-0.22	-0.22	-0.22	-0.22
105	-0.37	-0.37	-0.37	-0.37	-0.37	-0.37

Appendix 3.2

			Lift	Coefficient				
---------------------------------			REYNOLDS	NUMBER	------------------------			
ALPHA	80000	160000	360000	700000	1000000	2000000	5000000	10000000
0	0	0	0	0	0	0	0	0
1	0.11	0.11	0.11	0.11	0.11	0.11	0.11	0.11
2	0.22	0.22	0.22	0.22	0.22	0.22	0.22	0.22
3	0.33	0.33	0.33	0.33	0.33	0.33	0.33	0.33
4	0.4186	0.44	0.44	0.44	0.44	0.44	0.44	0.44
5	0.518	0.55	0.55	0.55	0.55	0.55	0.55	0.55
6	0.6048	0.6299	0.66	0.66	0.66	0.66	0.66	0.66
7	0.676	0.715	0.739	0.7483	0.77	0.77	0.77	0.77
8	0.7189	0.7851	0.824	0.8442	0.8504	0.88	0.88	0.88
9	0.6969	0.8311	0.8946	0.926	0.9387	0.9574	0.99	0.99
10	0.6122	0.8322	0.944	0.9937	1.0141	1.0433	1.0685	1.1
11	0.1642	0.7623	0.9572	1.0363	1.0686	1.1138	1.1553	1.1749
12	0.0749	0.5936	0.9285	1.0508	1.0971	1.1667	1.229	1.2591
13	0.0967	0.3548	0.8562	1.0302	1.0957	1.1948	1.2847	1.33
14	0.1382	0.2371	0.7483	0.9801	1.0656	1.1962	1.3187	1.3825
15	0.1861	0.2376	0.635	0.9119	1.0145	1.1744	1.3298	1.4136
16	0.2364	0.2665	0.5384	0.8401	0.9567	1.1356	1.3186	1.4233
17	0.2873	0.3098	0.4851	0.7799	0.8996	1.0921	1.2917	1.4136
18	0.3393	0.3567	0.4782	0.7305	0.8566	1.051	1.2576	1.3897
19	0.3927	0.4066	0.4908	0.7041	0.8226	1.0173	1.2242	1.3608
20	0.4463	0.4575	0.5247	0.699	0.8089	0.9954	1.1965	1.3325
21	0.5001	0.5087	0.5616	0.7097	0.8063	0.9837	1.1771	1.3077
22	0.5539	0.5611	0.6045	0.7298	0.8189	0.9827	1.1647	1.2767
23	0.6078	0.6148	0.6528	0.7593	0.8408	0.991	1.1611	1.1981
24	0.6617	0.6685	0.7015	0.7961	0.8668	1.0078	1.1563	1.1538
25	0.7156	0.7224	0.7511	0.8353	0.9023	1.0317	1.1322	1.138
26	0.77	0.7771	0.8055	0.8838	0.9406	1.0591	1.1268	1.1374
27	0.8277	0.8382	0.8788	0.9473	0.9912	1.081	1.1397	1.1519
30	0.855	0.855	0.93	0.96	1.01	1.07	1.1	1.12
35	0.98	0.98	0.982	0.98	1.02	1.062	1.08	1.1
40	1.035	1.035	1.035	1.035	1.035	1.055	1.06	1.07
45	1.05	1.05	1.05	1.05	1.05	1.05	1.05	1.05
50	1.02	1.02	1.02	1.02	1.02	1.02	1.02	1.02
55	0.955	0.955	0.955	0.955	0.955	0.955	0.955	0.955
60	0.875	0.875	0.875	0.875	0.875	0.875	0.875	0.875
65	0.76	0.76	0.76	0.76	0.76	0.76	0.76	0.76
70	0.63	0.63	0.63	0.63	0.63	0.63	0.63	0.63
75	0.5	0.5	0.5	0.5	0.5	0.5	0.5	0.5
80	0.365	0.365	0.365	0.365	0.365	0.365	0.365	0.365
85	0.23	0.23	0.23	0.23	0.23	0.23	0.23	0.23
90	0.09	0.09	0.09	0.09	0.09	0.09	0.09	0.09
95	-0.05	-0.05	-0.05	-0.05	-0.05	-0.05	-0.05	-0.05
100	-0.185	-0.185	-0.185	-0.185	-0.185	-0.185	-0.185	-0.185
105	-0.32	-0.32	-0.32	-0.32	-0.32	-0.32	-0.32	-0.32

Appendix 3.3

			Lift	Coefficient				
--------------------------------			REYNOLDS	NUMBER	-----------------------			
ALPHA	80000	160000	360000	700000	1000000	2000000	5000000	10000000
0	0	0	0	0	0	0	0	0
1	0.0936	0.0889	0.11	0.11	0.11	0.11	0.11	0.11
2	0.1833	0.1935	0.22	0.22	0.22	0.22	0.22	0.22
3	0.2688	0.2924	0.3088	0.33	0.33	0.33	0.33	0.33
4	0.3495	0.388	0.4114	0.44	0.44	0.44	0.44	0.44
5	0.4117	0.4753	0.5068	0.524	0.55	0.55	0.55	0.55
6	0.4573	0.5615	0.596	0.6228	0.6328	0.66	0.66	0.66
7	0.4758	0.6224	0.6724	0.71	0.7291	0.7362	0.7449	0.77
8	0.4428	0.6589	0.7373	0.7879	0.8156	0.8256	0.8439	0.8538
9	0.3544	0.6606	0.7781	0.8526	0.8904	0.9067	0.9314	0.9525
10	0.2108	0.6248	0.7949	0.8983	0.9541	0.9751	1.0111	1.0404
11	0.1124	0.5531	0.7852	0.9249	0.9973	1.0284	1.0772	1.1211
12	0.0139	0.4408	0.7488	0.9279	1.0245	1.0664	1.1296	1.1884
13	0.0314	0.3332	0.6923	0.9104	1.0289	1.0804	1.1662	1.243
14	0.0489	0.2256	0.6237	0.8803	1.0175	1.0793	1.1813	1.2808
15	0.0889	0.2142	0.5567	0.8405	0.9938	1.0624	1.1813	1.3004
16	0.1287	0.2027	0.4896	0.8007	0.9648	1.0402	1.1695	1.3067
17	0.1758	0.2315	0.4549	0.7663	0.9399	1.0181	1.155	1.3038
18	0.2228	0.2603	0.4202	0.7319	0.915	0.9959	1.1383	1.296
19	0.2732	0.3038	0.4292	0.7158	0.9014	0.9833	1.1278	1.2853
20	0.3236	0.3472	0.4382	0.6997	0.8877	0.9707	1.1172	1.2768
21	0.3751	0.3951	0.4704	0.7024	0.8872	0.9702	1.115	1.2741
22	0.4265	0.443	0.5026	0.705	0.8867	0.9696	1.1127	1.2714
25	0.584	0.5963	0.6321	0.7724	0.9326	1.0107	1.1468	1.2925
30	0.855	0.855	0.855	0.855	0.855	0.855	0.855	0.855
35	0.98	0.98	0.98	0.98	0.98	0.98	0.98	0.98
40	1.035	1.035	1.035	1.035	1.035	1.035	1.035	1.035
45	1.05	1.05	1.05	1.05	1.05	1.05	1.05	1.05
50	1.02	1.02	1.02	1.02	1.02	1.02	1.02	1.02
55	0.955	0.955	0.955	0.955	0.955	0.955	0.955	0.955
60	0.875	0.875	0.875	0.875	0.875	0.875	0.875	0.875
65	0.76	0.76	0.76	0.76	0.76	0.76	0.76	0.76
70	0.63	0.63	0.63	0.63	0.63	0.63	0.63	0.63
75	0.5	0.5	0.5	0.5	0.5	0.5	0.5	0.5
80	0.365	0.365	0.365	0.365	0.365	0.365	0.365	0.365
85	0.23	0.23	0.23	0.23	0.23	0.23	0.23	0.23
90	0.09	0.09	0.09	0.09	0.09	0.09	0.09	0.09
95	-0.05	-0.05	-0.05	-0.05	-0.05	-0.05	-0.05	-0.05
100	-0.185	-0.185	-0.185	-0.185	-0.185	-0.185	-0.185	-0.185
105	-0.32	-0.32	-0.32	-0.32	-0.32	-0.32	-0.32	-0.32
110	-0.45	-0.45	-0.45	-0.45	-0.45	-0.45	-0.45	-0.45
115	-0.575	-0.575	-0.575	-0.575	-0.575	-0.575	-0.575	-0.575
120	-0.67	-0.67	-0.67	-0.67	-0.67	-0.67	-0.67	-0.67
125	-0.76	-0.76	-0.76	-0.76	-0.76	-0.76	-0.76	-0.76

Appendix 3.4

			Lift	Coefficient				
--------------------------------			REYNOLDS	NUMBER	-----------------------			
ALPHA	80000	160000	360000	700000	1000000	2000000	5000000	10000000
0	0	0	0	0	0	0	0	0
1	0.0752	0.0921	0.0842	0.11	0.11	0.11	0.11	0.11
2	0.1465	0.1839	0.1879	0.22	0.22	0.22	0.22	0.22
3	0.2103	0.2731	0.2861	0.3024	0.33	0.33	0.33	0.33
4	0.273	0.3564	0.38	0.4044	0.4128	0.44	0.44	0.44
5	0.3086	0.4324	0.4687	0.4998	0.5146	0.5192	0.55	0.55
6	0.3382	0.4953	0.5486	0.5891	0.61	0.6191	0.6268	0.66
7	0.3427	0.5445	0.6209	0.6728	0.6988	0.7102	0.7254	0.7354
8	0.342	0.5751	0.6745	0.7434	0.7802	0.7939	0.8143	0.8334
9	0.3162	0.5874	0.7148	0.8026	0.8498	0.8694	0.8986	0.9222
10	0.2691	0.578	0.7374	0.85	0.9091	0.9364	0.9739	1.0049
11	0.2176	0.5564	0.7443	0.8779	0.9543	0.9862	1.0398	1.0787
12	0.166	0.5228	0.7363	0.8938	0.9843	1.0257	1.0906	1.1453
13	0.1247	0.4762	0.7255	0.8973	1.002	1.0492	1.1305	1.1979
14	0.0833	0.4296	0.6993	0.8937	1.0122	1.0657	1.158	1.241
15	0.0907	0.3898	0.674	0.884	1.0106	1.0709	1.1747	1.268
16	0.0981	0.3499	0.6487	0.8717	1.0056	1.069	1.1823	1.286
17	0.13	0.336	0.6293	0.8603	0.9973	1.0641	1.1824	1.2977
18	0.1619	0.3221	0.6098	0.8489	0.9911	1.0588	1.1814	1.3031
19	0.2017	0.3348	0.6009	0.8443	0.9885	1.0571	1.1797	1.3066
20	0.2414	0.3475	0.592	0.8397	0.9858	1.0554	1.1812	1.3054
21	0.288	0.3783	0.5972	0.8425	0.9899	1.0599	1.1853	1.3092
22	0.3345	0.4091	0.6023	0.8453	0.994	1.0644	1.1893	1.313
25	0.4802	0.5297	0.6664	0.8866	1.035	1.1018	1.223	1.3476
30	0.855	0.855	0.855	0.855	0.855	0.855	0.855	0.855
35	0.98	0.98	0.98	0.98	0.98	0.98	0.98	0.98
40	1.035	1.035	1.035	1.035	1.035	1.035	1.035	1.035
45	1.05	1.05	1.05	1.05	1.05	1.05	1.05	1.05
50	1.02	1.02	1.02	1.02	1.02	1.02	1.02	1.02
55	0.955	0.955	0.955	0.955	0.955	0.955	0.955	0.955
60	0.875	0.875	0.875	0.875	0.875	0.875	0.875	0.875
65	0.76	0.76	0.76	0.76	0.76	0.76	0.76	0.76
70	0.63	0.63	0.63	0.63	0.63	0.63	0.63	0.63
75	0.5	0.5	0.5	0.5	0.5	0.5	0.5	0.5
80	0.365	0.365	0.365	0.365	0.365	0.365	0.365	0.365
85	0.23	0.23	0.23	0.23	0.23	0.23	0.23	0.23
90	0.09	0.09	0.09	0.09	0.09	0.09	0.09	0.09
95	-0.05	-0.05	-0.05	-0.05	-0.05	-0.05	-0.05	-0.05
100	-0.185	-0.185	-0.185	-0.185	-0.185	-0.185	-0.185	-0.185
105	-0.32	-0.32	-0.32	-0.32	-0.32	-0.32	-0.32	-0.32
110	-0.45	-0.45	-0.45	-0.45	-0.45	-0.45	-0.45	-0.45
115	-0.575	-0.575	-0.575	-0.575	-0.575	-0.575	-0.575	-0.575
120	-0.67	-0.67	-0.67	-0.67	-0.67	-0.67	-0.67	-0.67
125	-0.76	-0.76	-0.76	-0.76	-0.76	-0.76	-0.76	-0.76

Appendix 3.5

		Drag	Coefficient		NACA0012	
-------------------------------			REYNOLDS	NUMBER	-----------------------	
ALPHA	160000	360000	700000	1000000	2000000	5000000
0	0.0103	0.0079	0.0067	0.0065	0.0064	0.0064
1	0.0104	0.008	0.0068	0.0066	0.0064	0.0064
2	0.0108	0.0084	0.007	0.0068	0.0066	0.0066
3	0.0114	0.0089	0.0075	0.0071	0.0069	0.0068
4	0.0124	0.0098	0.0083	0.0078	0.0073	0.0072
5	0.014	0.0113	0.0097	0.0091	0.0081	0.0076
6	0.0152	0.0125	0.0108	0.0101	0.009	0.0081
7	0.017	0.0135	0.0118	0.011	0.0097	0.0086
8	0.0185	0.0153	0.0128	0.0119	0.0105	0.0092
9	0.0203	0.0167	0.0144	0.0134	0.0113	0.0098
10	0.0188	0.0184	0.0159	0.0147	0.0128	0.0106
11	0.076	0.0204	0.0175	0.0162	0.014	0.0118
12	0.134	0.0217	0.0195	0.018	0.0155	0.013
13	0.152	0.0222	0.0216	0.02	0.0172	0.0143
14	0.171	0.106	0.0236	0.0222	0.0191	0.0159
15	0.19	0.19	0.117	0.0245	0.0213	0.0177
16	0.21	0.21	0.21	0.128	0.0237	0.0198
17	0.231	0.231	0.23	0.231	0.138	0.0229
18	0.252	0.252	0.252	0.252	0.252	0.148
19	0.274	0.274	0.274	0.274	0.274	0.274
20	0.297	0.297	0.297	0.297	0.297	0.297
21	0.32	0.32	0.32	0.32	0.32	0.32
22	0.344	0.344	0.344	0.344	0.344	0.344
23	0.369	0.369	0.369	0.369	0.369	0.369
24	0.394	0.394	0.394	0.394	0.394	0.394
25	0.42	0.42	0.42	0.42	0.42	0.42
26	0.446	0.446	0.446	0.446	0.446	0.446
27	0.473	0.473	0.473	0.473	0.473	0.473
30	0.57	0.57	0.57	0.57	0.57	0.57
35	0.745	0.745	0.745	0.745	0.745	0.745
40	0.92	0.92	0.92	0.92	0.92	0.92
45	1.075	1.075	1.075	1.075	1.075	1.075
50	1.215	1.215	1.215	1.215	1.215	1.215
55	1.345	1.345	1.345	1.345	1.345	1.345
60	1.47	1.47	1.47	1.47	1.47	1.47
65	1.575	1.575	1.575	1.575	1.575	1.575
70	1.665	1.665	1.665	1.665	1.665	1.665
75	1.735	1.735	1.735	1.735	1.735	1.735
80	1.78	1.78	1.78	1.78	1.78	1.78
85	1.8	1.8	1.8	1.8	1.8	1.8
90	1.8	1.8	1.8	1.8	1.8	1.8
95	1.78	1.78	1.78	1.78	1.78	1.78
100	1.75	1.75	1.75	1.75	1.75	1.75

Appendix 3.6

	Drag		Coefficient					
--------------------------------			REYNOLDS	NUMBER	-----------------------			
ALPHA	80000	160000	360000	700000	1000000	2000000	5000000	10000000
0	0.0147	0.0116	0.0091	0.0077	0.0074	0.007	0.0068	0.0068
1	0.0148	0.0117	0.0092	0.0078	0.0075	0.0071	0.0069	0.0068
2	0.0151	0.012	0.0094	0.008	0.0076	0.0072	0.007	0.0069
3	0.0156	0.0124	0.0098	0.0083	0.0079	0.0075	0.0073	0.0071
4	0.0168	0.0132	0.0105	0.0089	0.0083	0.0078	0.0075	0.0074
5	0.0181	0.0142	0.0114	0.0098	0.0091	0.0083	0.008	0.0077
6	0.0197	0.016	0.0126	0.0108	0.0101	0.009	0.0084	0.0081
7	0.0214	0.0176	0.0143	0.0122	0.0111	0.0098	0.0089	0.0086
8	0.0234	0.0193	0.0157	0.0135	0.0126	0.0108	0.0095	0.009
9	0.0255	0.0212	0.0173	0.0149	0.0138	0.0121	0.0102	0.0096
10	0.0277	0.0233	0.0191	0.0164	0.0152	0.0133	0.0113	0.0103
11	0.076	0.0256	0.0211	0.0182	0.0168	0.0146	0.0124	0.0114
12	0.123	0.0281	0.0233	0.02	0.0186	0.0161	0.0136	0.0123
13	0.14	0.0302	0.0257	0.0221	0.0205	0.0177	0.0149	0.0134
14	0.158	0.104	0.0283	0.0244	0.0225	0.0195	0.0164	0.0147
15	0.177	0.177	0.0312	0.0269	0.0249	0.0215	0.018	0.0161
16	0.196	0.197	0.124	0.0297	0.0275	0.0237	0.0198	0.0176
17	0.217	0.217	0.217	0.134	0.0303	0.0261	0.0218	0.0194
18	0.238	0.238	0.238	0.238	0.145	0.0288	0.024	0.0213
19	0.26	0.26	0.26	0.26	0.26	0.155	0.0265	0.0234
20	0.282	0.282	0.282	0.282	0.282	0.282	0.166	0.0257
21	0.305	0.305	0.305	0.305	0.305	0.305	0.305	0.177
22	0.329	0.329	0.329	0.329	0.329	0.329	0.329	0.329
23	0.354	0.354	0.354	0.354	0.354	0.354	0.354	0.354
24	0.379	0.379	0.379	0.379	0.379	0.379	0.379	0.379
25	0.405	0.405	0.405	0.405	0.405	0.405	0.405	0.405
26	0.432	0.432	0.432	0.432	0.432	0.432	0.432	0.432
27	0.46	0.46	0.46	0.46	0.46	0.46	0.46	0.46
30	0.57	0.57	0.57	0.57	0.57	0.57	0.57	0.57
35	0.745	0.745	0.745	0.745	0.745	0.745	0.745	0.745
40	0.92	0.92	0.92	0.92	0.92	0.92	0.92	0.92
45	1.075	1.075	1.075	1.075	1.075	1.075	1.075	1.075
50	1.215	1.215	1.215	1.215	1.215	1.215	1.215	1.215
55	1.345	1.345	1.345	1.345	1.345	1.345	1.345	1.345
60	1.47	1.47	1.47	1.47	1.47	1.47	1.47	1.47
65	1.575	1.575	1.575	1.575	1.575	1.575	1.575	1.575
70	1.665	1.665	1.665	1.665	1.665	1.665	1.665	1.665
75	1.735	1.735	1.735	1.735	1.735	1.735	1.735	1.735
80	1.78	1.78	1.78	1.78	1.78	1.78	1.78	1.78
85	1.8	1.8	1.8	1.8	1.8	1.8	1.8	1.8
90	1.8	1.8	1.8	1.8	1.8	1.8	1.8	1.8
95	1.78	1.78	1.78	1.78	1.78	1.78	1.78	1.78
100	1.75	1.75	1.75	1.75	1.75	1.75	1.75	1.75
105	1.7	1.7	1.7	1.7	1.7	1.7	1.7	1.7

Appendix 3.7

	Drag		Coefficient					
--------------------------------			REYNOLDS NUMBER		-----------------------			
ALPHA	80000	160000	360000	700000	1000000	2000000	5000000	10000000
0	0.0214	0.0162	0.0128	0.0101	0.0085	0.0082	0.0077	0.0073
1	0.0215	0.0163	0.0129	0.0102	0.0087	0.0082	0.0077	0.0073
2	0.0219	0.0167	0.0131	0.0104	0.0088	0.0083	0.0078	0.0075
3	0.0225	0.0172	0.0137	0.0107	0.0091	0.0086	0.008	0.0077
4	0.0235	0.0181	0.0144	0.0112	0.0096	0.0089	0.0084	0.0079
5	0.0247	0.0192	0.0153	0.0121	0.0102	0.0095	0.0087	0.0083
6	0.0263	0.0206	0.0166	0.0132	0.0112	0.0102	0.0093	0.0087
7	0.0282	0.0223	0.0181	0.0145	0.0123	0.0115	0.0101	0.0093
8	0.0303	0.0242	0.0198	0.0159	0.0136	0.0126	0.0111	0.01
9	0.0327	0.0264	0.0217	0.0176	0.015	0.0139	0.0122	0.0108
10	0.062	0.0288	0.0238	0.0194	0.0166	0.0154	0.0134	0.0117
11	0.0925	0.0315	0.0262	0.0213	0.0183	0.017	0.0148	0.0128
12	0.123	0.08	0.0288	0.0235	0.0202	0.0187	0.0163	0.014
13	0.1405	0.119	0.077	0.0259	0.0223	0.0206	0.0179	0.0153
14	0.158	0.158	0.158	0.094	0.0245	0.0227	0.0197	0.0168
15	0.177	0.177	0.177	0.145	0.102	0.0251	0.0218	0.0185
16	0.196	0.196	0.196	0.196	0.196	0.108	0.024	0.0203
17	0.217	0.217	0.217	0.217	0.217	0.173	0.12	0.0223
18	0.238	0.238	0.238	0.238	0.238	0.238	0.238	0.0244
19	0.26	0.26	0.26	0.26	0.26	0.26	0.26	0.14
20	0.282	0.282	0.282	0.282	0.282	0.282	0.282	0.282
21	0.3055	0.3055	0.3055	0.3055	0.3055	0.3055	0.3055	0.3055
22	0.329	0.329	0.329	0.329	0.329	0.329	0.329	0.329
25	0.405	0.405	0.405	0.405	0.405	0.405	0.405	0.405
30	0.57	0.57	0.57	0.57	0.57	0.57	0.57	0.57
35	0.745	0.745	0.745	0.745	0.745	0.745	0.745	0.745
40	0.92	0.92	0.92	0.92	0.92	0.92	0.92	0.92
45	1.075	1.075	1.075	1.075	1.075	1.075	1.075	1.075
50	1.215	1.215	1.215	1.215	1.215	1.215	1.215	1.215
55	1.345	1.345	1.345	1.345	1.345	1.345	1.345	1.345
60	1.47	1.47	1.47	1.47	1.47	1.47	1.47	1.47
65	1.575	1.575	1.575	1.575	1.575	1.575	1.575	1.575
70	1.665	1.665	1.665	1.665	1.665	1.665	1.665	1.665
75	1.735	1.735	1.735	1.735	1.735	1.735	1.735	1.735
80	1.78	1.78	1.78	1.78	1.78	1.78	1.78	1.78
85	1.8	1.8	1.8	1.8	1.8	1.8	1.8	1.8
90	1.8	1.8	1.8	1.8	1.8	1.8	1.8	1.8
95	1.78	1.78	1.78	1.78	1.78	1.78	1.78	1.78
100	1.75	1.75	1.75	1.75	1.75	1.75	1.75	1.75
105	1.7	1.7	1.7	1.7	1.7	1.7	1.7	1.7
110	1.635	1.635	1.635	1.635	1.635	1.635	1.635	1.635
115	1.555	1.555	1.555	1.555	1.555	1.555	1.555	1.555
120	1.465	1.465	1.465	1.465	1.465	1.465	1.465	1.465
125	1.35	1.35	1.35	1.35	1.35	1.35	1.35	1.35

Appendix 3.8

	Drag		Coefficient					
--------------------------------			REYNOLDS	NUMBER	-----------------------			
ALPHA	80000	160000	360000	700000	1000000	2000000	5000000	10000000
0	0.0232	0.0177	0.0139	0.0111	0.0094	0.0089	0.0082	0.0078
1	0.0233	0.0178	0.014	0.0111	0.0094	0.0089	0.0083	0.0078
2	0.0237	0.0181	0.0143	0.0113	0.0096	0.009	0.0084	0.0079
3	0.0243	0.0186	0.0148	0.0117	0.0098	0.0092	0.0086	0.0081
4	0.0253	0.0194	0.0155	0.0122	0.0103	0.0096	0.0089	0.0083
5	0.0264	0.0204	0.0163	0.0129	0.0109	0.0101	0.0092	0.0086
6	0.0279	0.0217	0.0174	0.0138	0.0117	0.0108	0.0098	0.0091
7	0.0297	0.0233	0.0187	0.0149	0.0126	0.0117	0.0105	0.0097
8	0.0319	0.0252	0.0204	0.0163	0.0138	0.0128	0.0114	0.0104
9	0.0343	0.0273	0.0222	0.0178	0.0152	0.014	0.0124	0.0112
10	0.062	0.0297	0.0243	0.0195	0.0166	0.0154	0.0135	0.0121
11	0.0925	0.07	0.0266	0.0215	0.0184	0.017	0.0148	0.0132
12	0.123	0.123	0.0292	0.0237	0.0202	0.0187	0.0162	0.0143
13	0.1405	0.1405	0.086	0.026	0.0223	0.0206	0.0179	0.0156
14	0.158	0.158	0.158	0.0286	0.0244	0.0226	0.0196	0.017
15	0.177	0.177	0.177	0.104	0.0269	0.0248	0.0215	0.0186
16	0.196	0.196	0.196	0.196	0.0295	0.0273	0.0236	0.0205
17	0.217	0.217	0.217	0.217	0.125	0.03	0.026	0.0224
18	0.238	0.238	0.238	0.238	0.238	0.135	0.0285	0.0245
19	0.26	0.26	0.26	0.26	0.26	0.2085	0.145	0.0268
20	0.282	0.282	0.282	0.282	0.282	0.282	0.282	0.0293
21	0.3055	0.3055	0.3055	0.3055	0.3055	0.3055	0.3055	0.1792
22	0.329	0.329	0.329	0.329	0.329	0.329	0.329	0.329
25	0.405	0.405	0.405	0.405	0.405	0.405	0.405	0.405
30	0.57	0.57	0.57	0.57	0.57	0.57	0.57	0.57
35	0.745	0.745	0.745	0.745	0.745	0.745	0.745	0.745
40	0.92	0.92	0.92	0.92	0.92	0.92	0.92	0.92
45	1.075	1.075	1.075	1.075	1.075	1.075	1.075	1.075
50	1.215	1.215	1.215	1.215	1.215	1.215	1.215	1.215
55	1.345	1.345	1.345	1.345	1.345	1.345	1.345	1.345
60	1.47	1.47	1.47	1.47	1.47	1.47	1.47	1.47
65	1.575	1.575	1.575	1.575	1.575	1.575	1.575	1.575
70	1.665	1.665	1.665	1.665	1.665	1.665	1.665	1.665
75	1.735	1.735	1.735	1.735	1.735	1.735	1.735	1.735
80	1.78	1.78	1.78	1.78	1.78	1.78	1.78	1.78
85	1.8	1.8	1.8	1.8	1.8	1.8	1.8	1.8
90	1.8	1.8	1.8	1.8	1.8	1.8	1.8	1.8
95	1.78	1.78	1.78	1.78	1.78	1.78	1.78	1.78
100	1.75	1.75	1.75	1.75	1.75	1.75	1.75	1.75
105	1.7	1.7	1.7	1.7	1.7	1.7	1.7	1.7
110	1.635	1.635	1.635	1.635	1.635	1.635	1.635	1.635
115	1.555	1.555	1.555	1.555	1.555	1.555	1.555	1.555
120	1.465	1.465	1.465	1.465	1.465	1.465	1.465	1.465
125	1.35	1.35	1.35	1.35	1.35	1.35	1.35	1.35

Figure 1

Click here to download high resolution image

FRANCIS EMEJEAMARA

FIGURE 1 TOP OF PAGE

Leeds

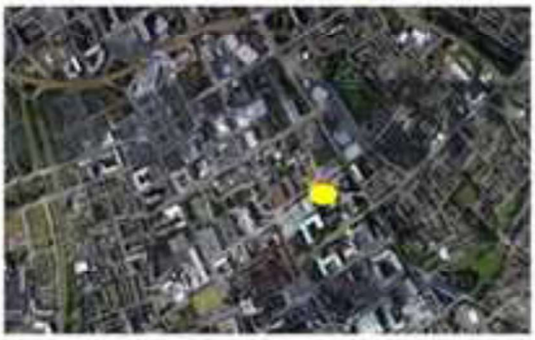

Manchester

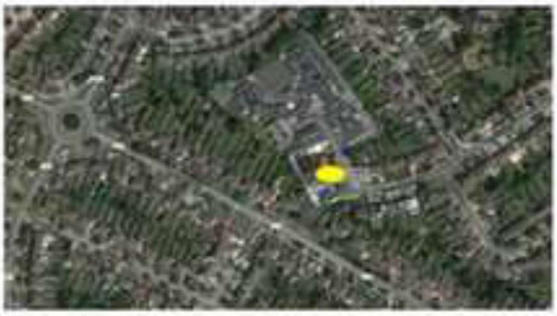

Dublin (St Pius)

Dublin (Marrowbone)

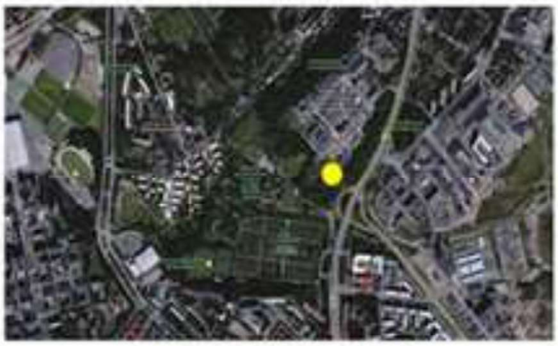

Helsinki (Suburban)

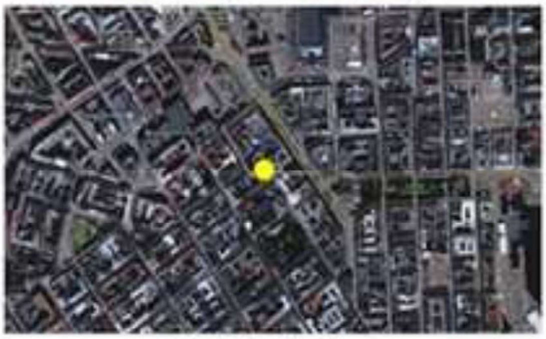

Helsinki (Urban)

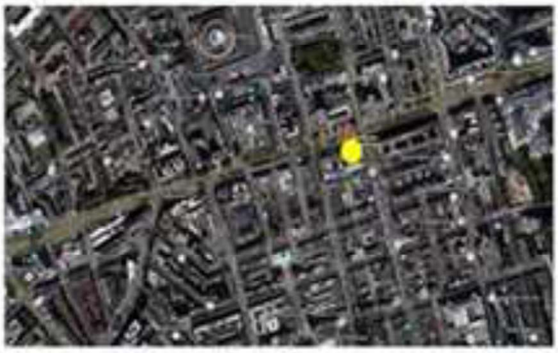

London

Figure 2
Click here to download high resolution image

FRANCIS EMEJEAMARA
FIGURE 2 TOP OF PAGE

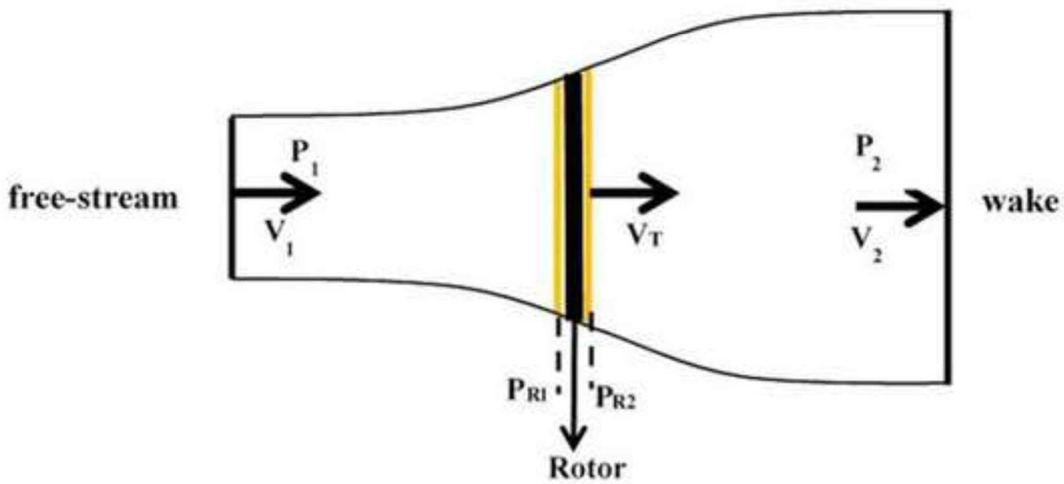

Figure 3
Click here to download high resolution image

FRANCIS EMEJEAMARA
FIGURE 3 TOP OF PAGE

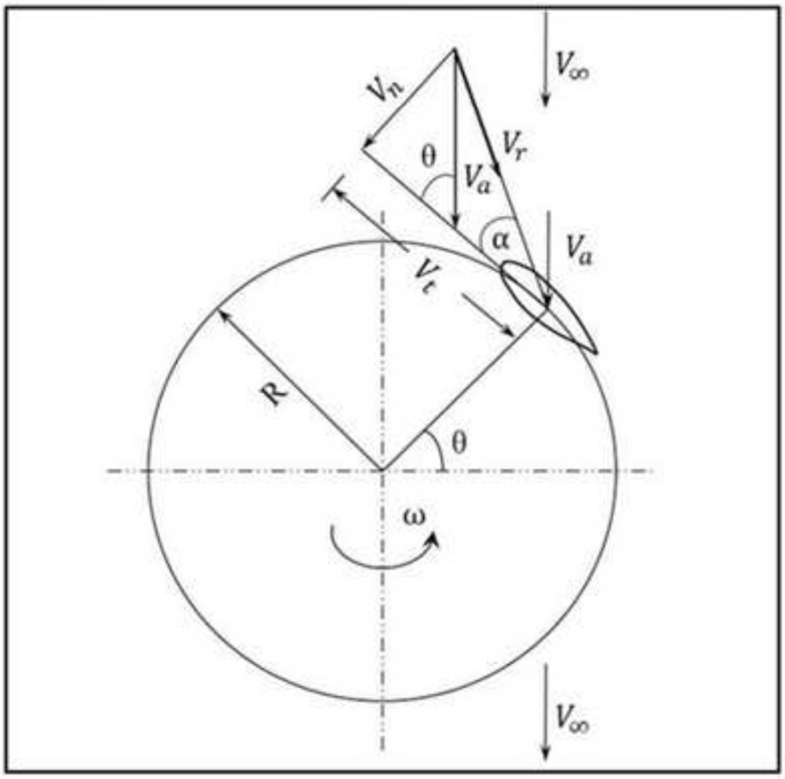

Figure 4
Click here to download high resolution image

FRANCIS EMEJEAMARA

FIGURE 4 TOP OF PAGE

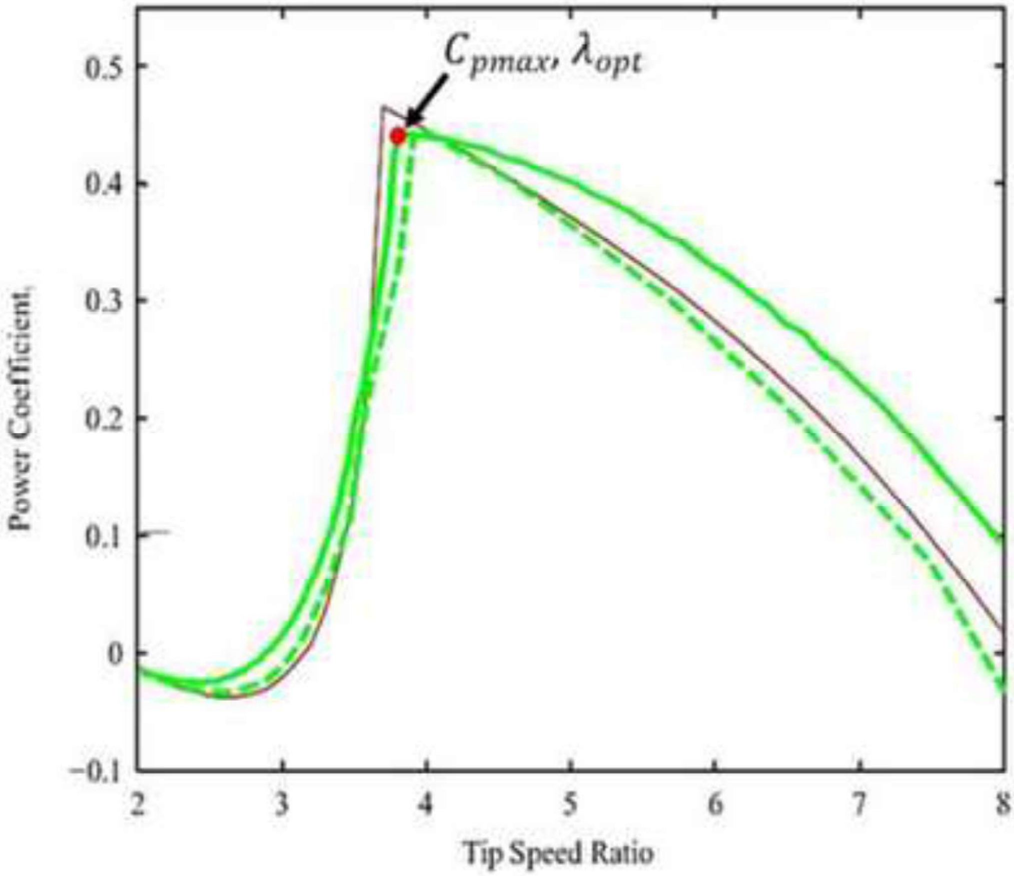

Figure 5
Click here to download high resolution image

FRANCIS EMEJEAMARA
FIGURE 5 TOP OF PAGE

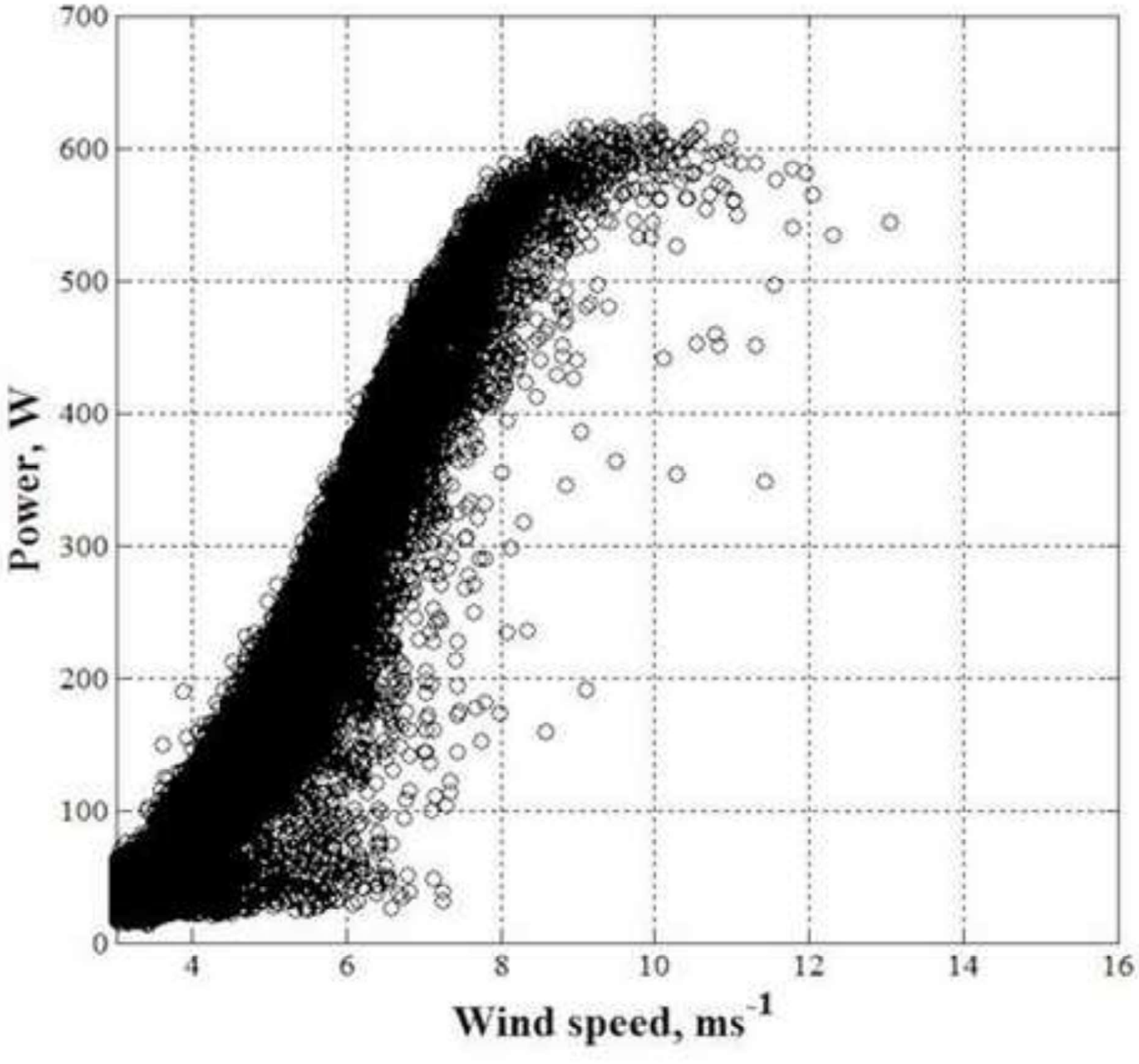

Figure 6
Click here to download high resolution image

FRANCIS EMEJEAMARA
FIGURE 6 TOP OF PAGE

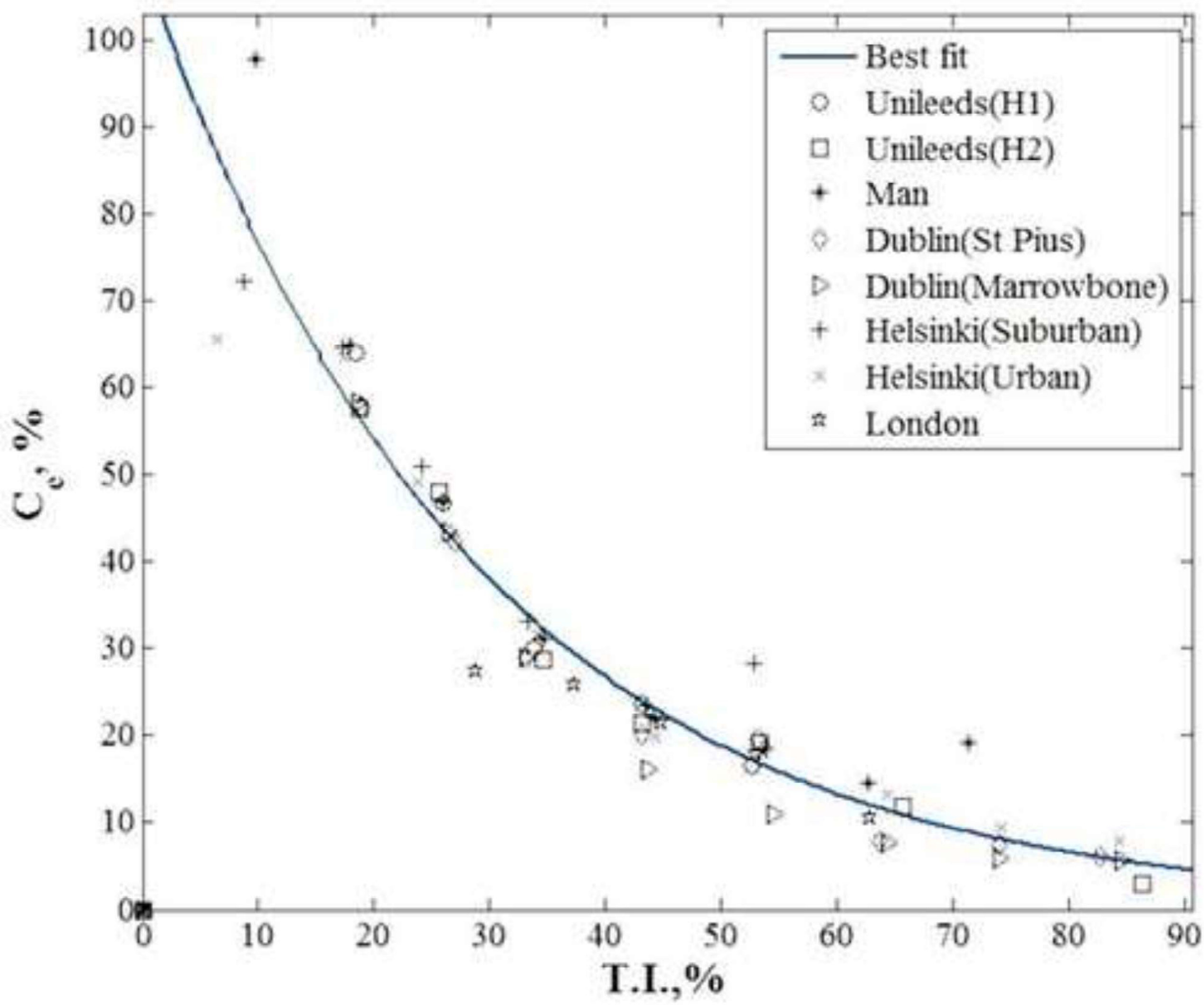

Figure 7
Click here to download high resolution image

FRANCIS EMEJEAMARA
FIGURE 7 TOP OF PAGE

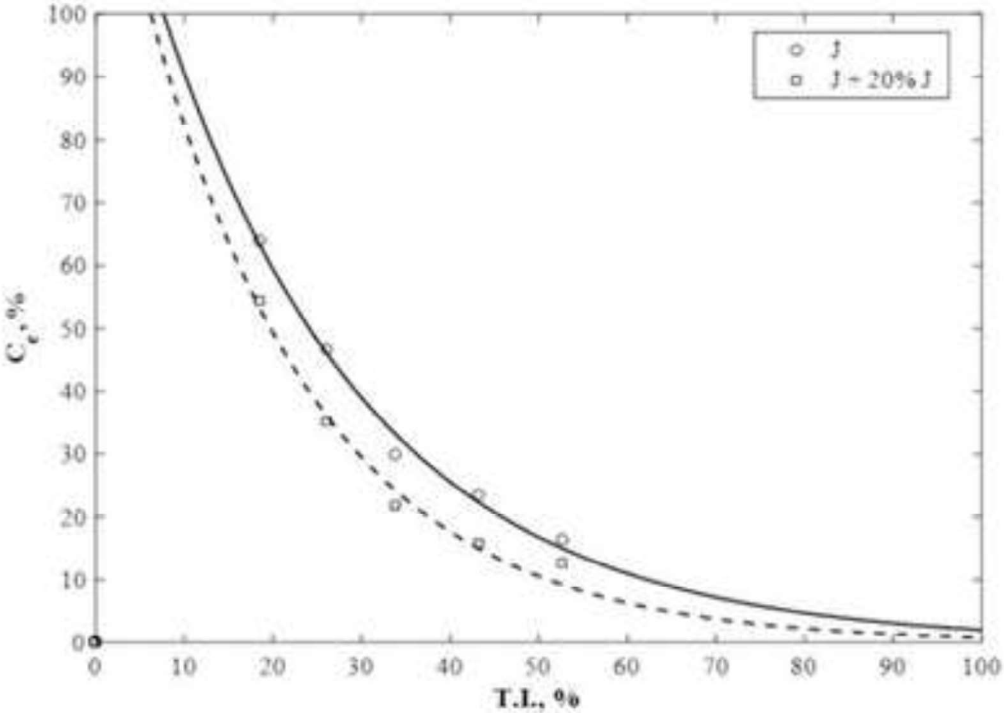

Figure 8
Click here to download high resolution image

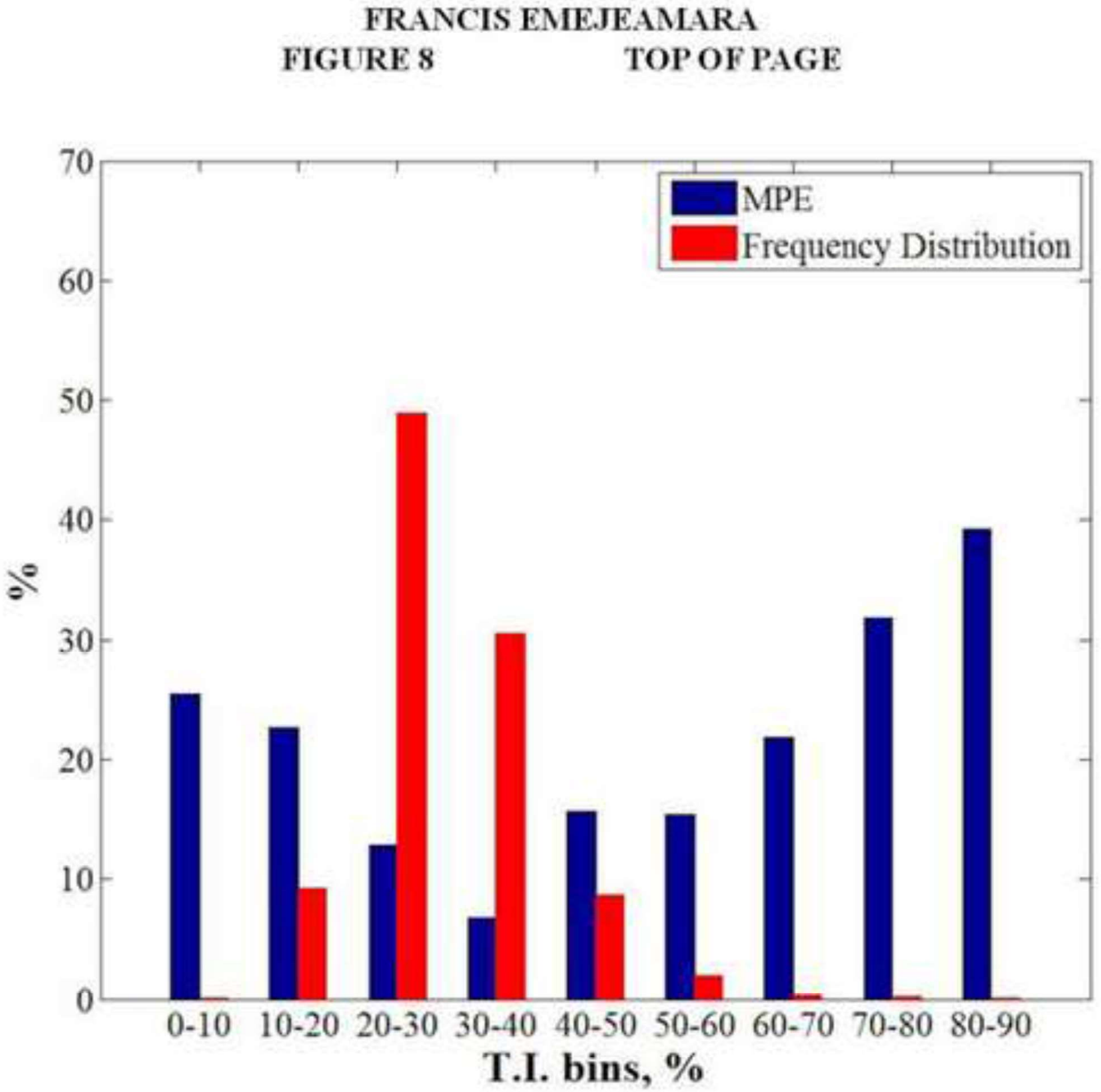

Figure 9
Click here to download high resolution image

FRANCIS EMEJEAMARA
FIGURE 9 TOP OF PAGE

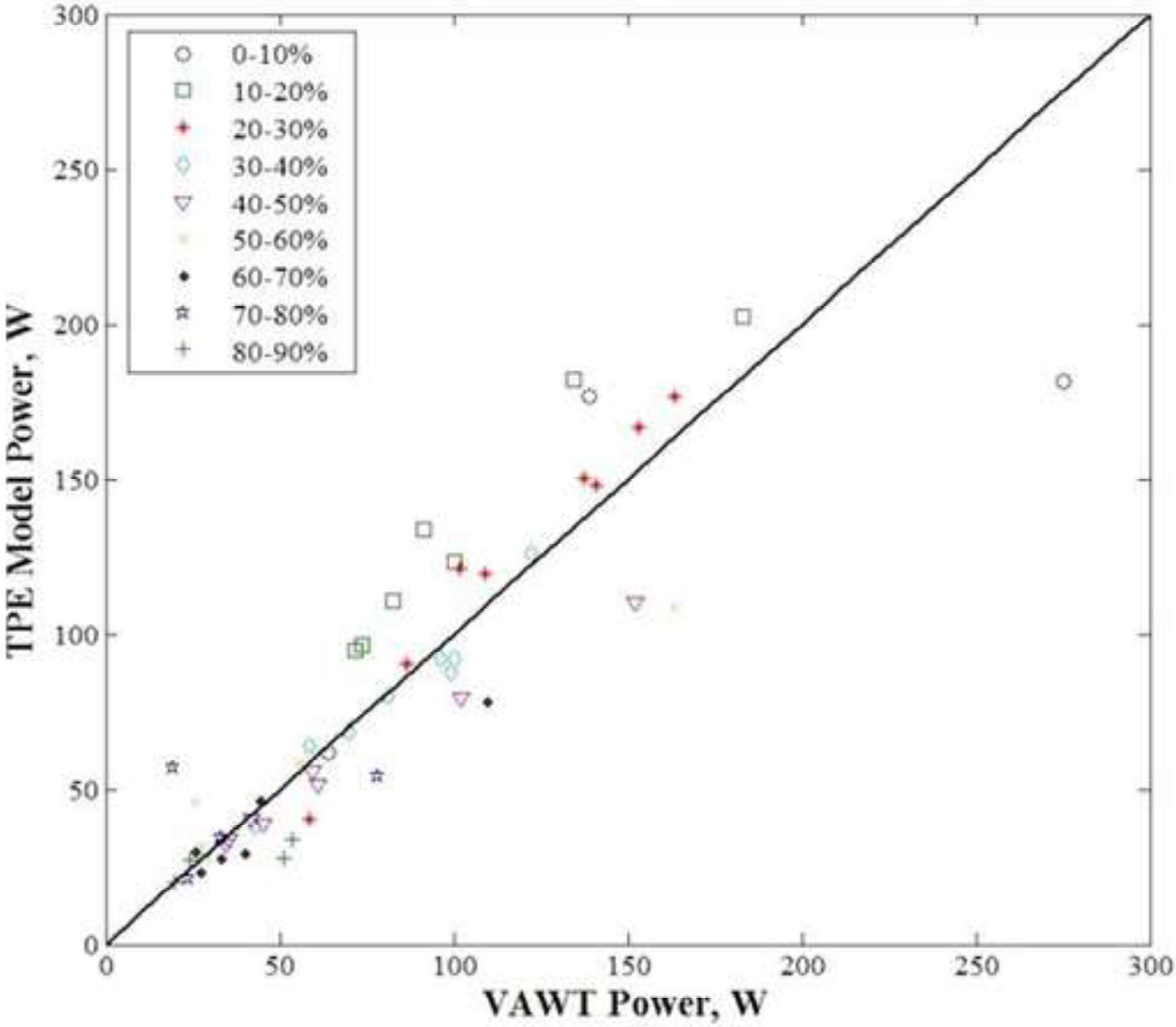

Figure 10
Click here to download high resolution image

FRANCIS EMEJEAMARA

FIGURE 10 TOP OF PAGE

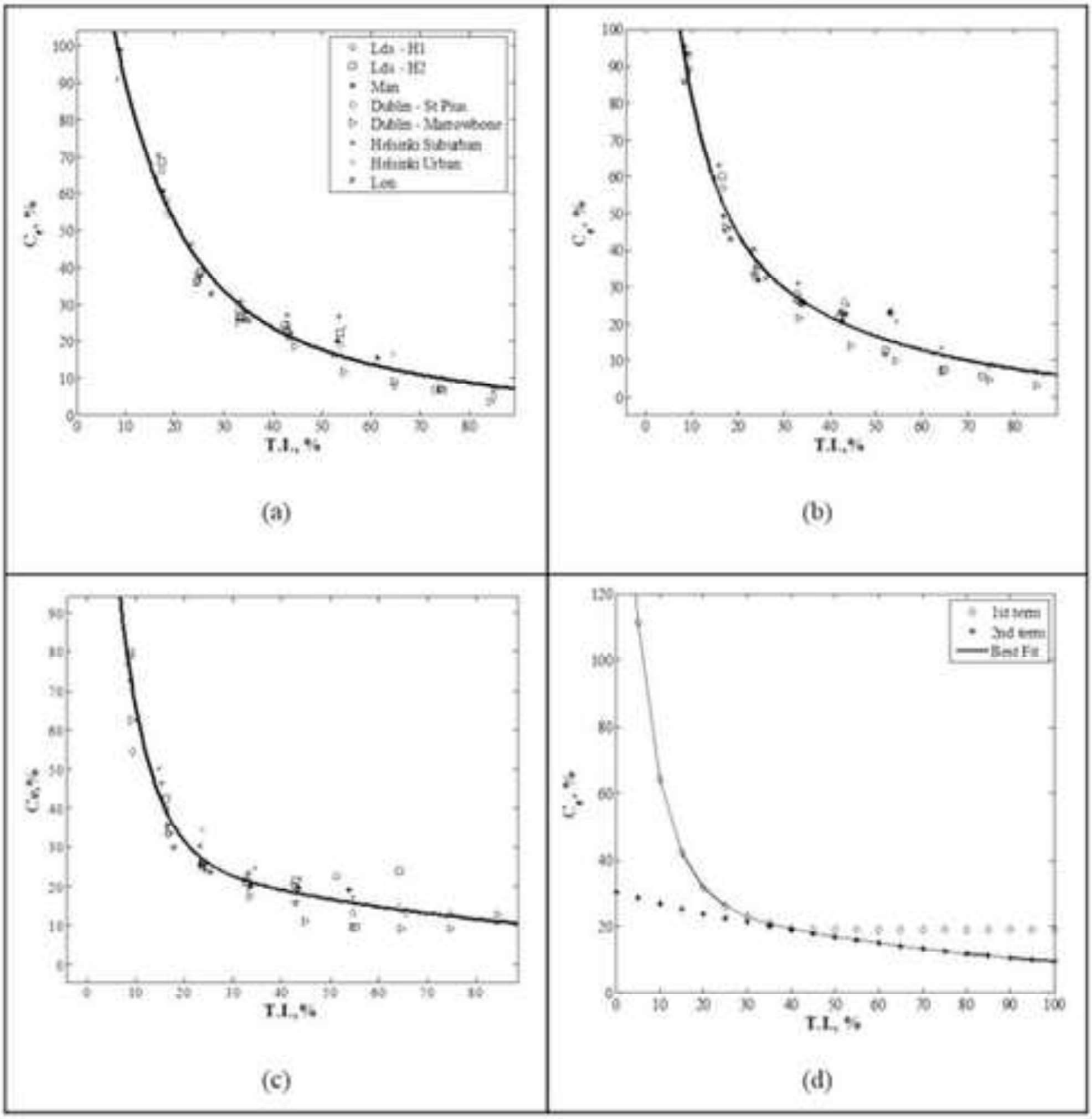

Figure 11
Click here to download high resolution image

FRANCIS EMEJEAMARA
FIGURE 11 TOP OF PAGE

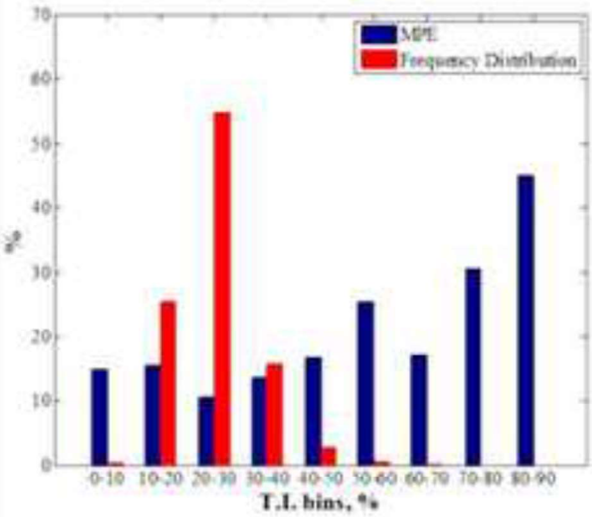

(a)

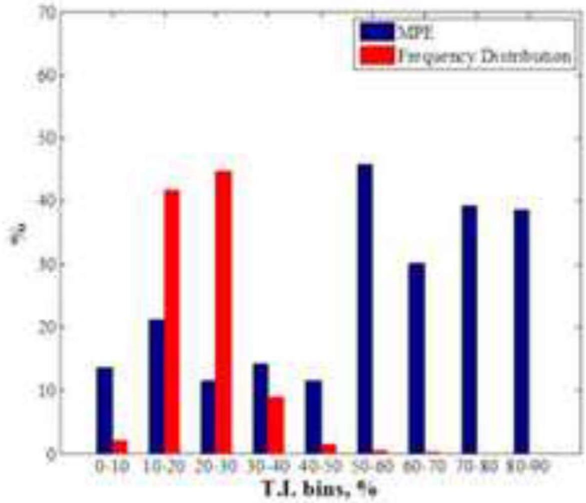

(b)

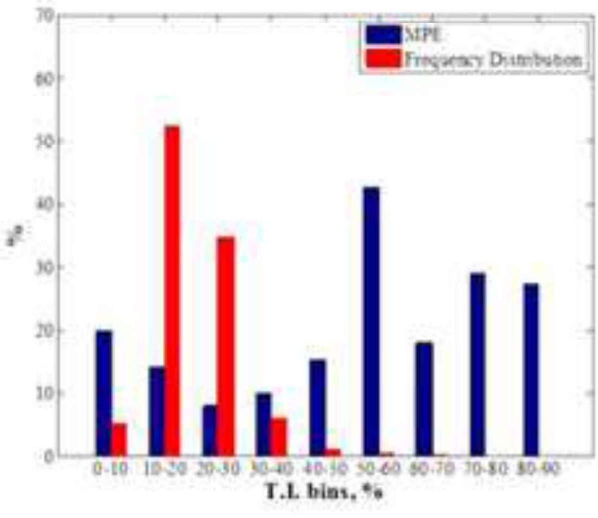

(c)

Figure 12
Click here to download high resolution image

FRANCIS EMEJEAMARA
FIGURE 12 TOP OF PAGE

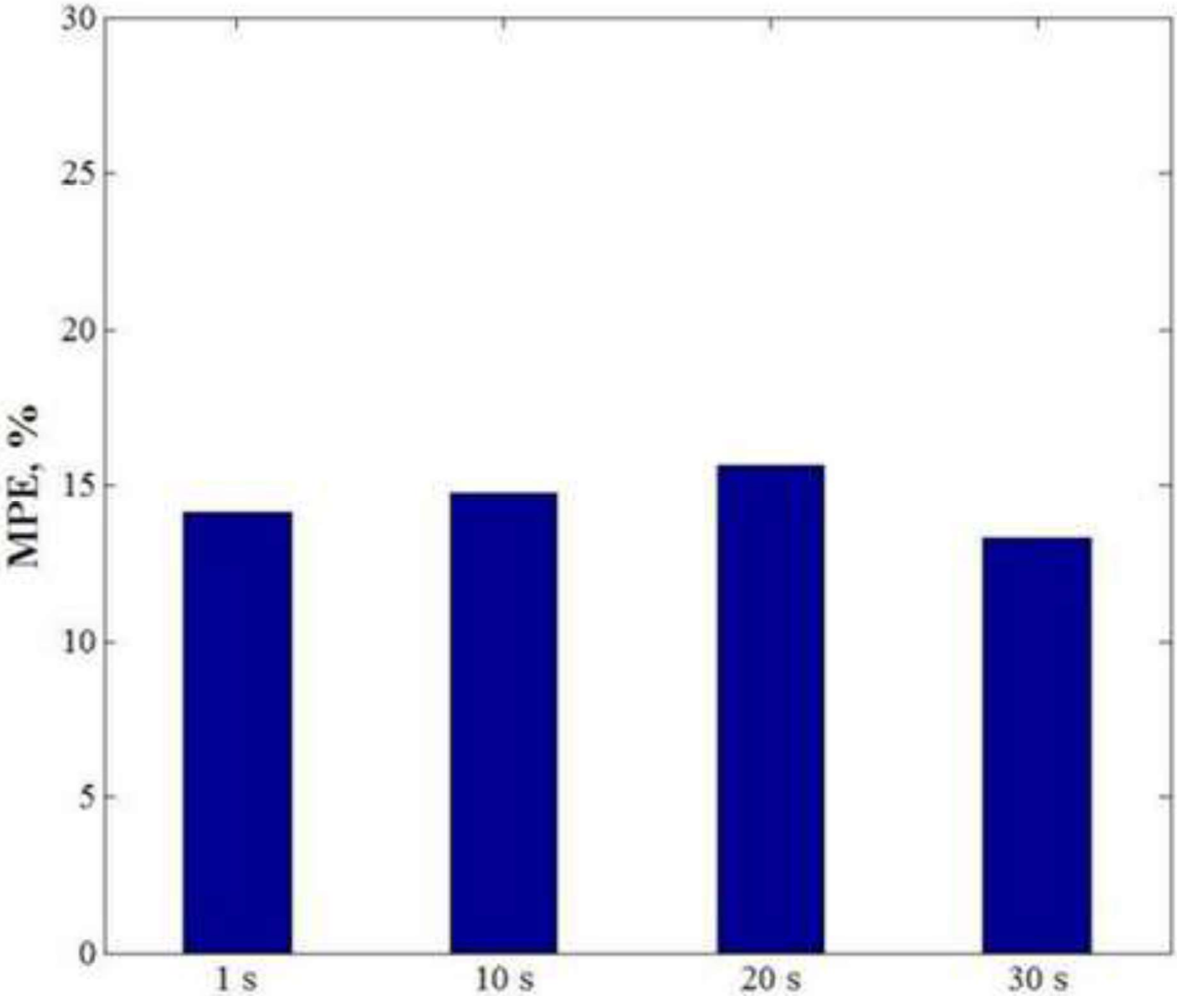

Appendix 1

FRANCIS EMEJEAMARA

APPENDIX 1 TOP OF PAGE

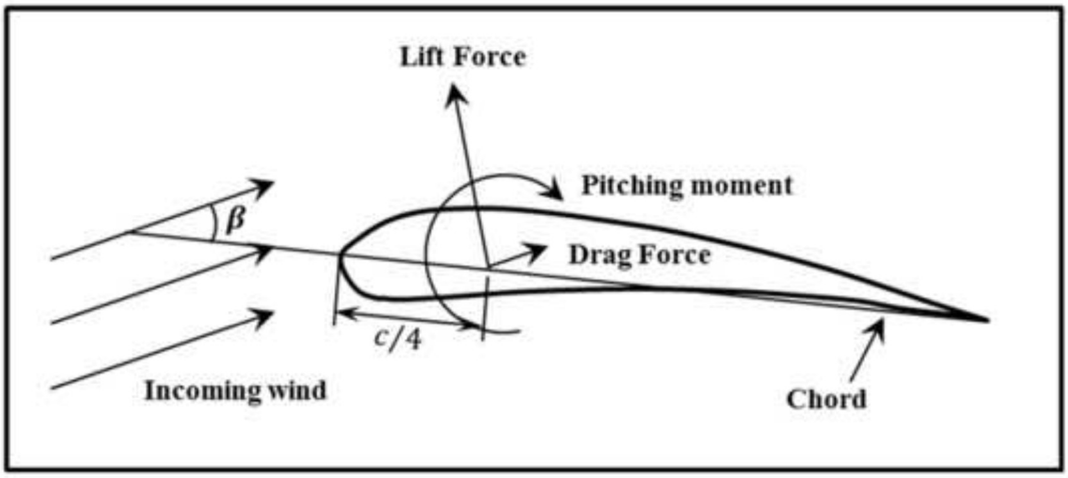

Appendix 2

Click here to download high resolution image

FRANCIS EMEJEAMARA

APPENDIX 2 TOP OF PAGE

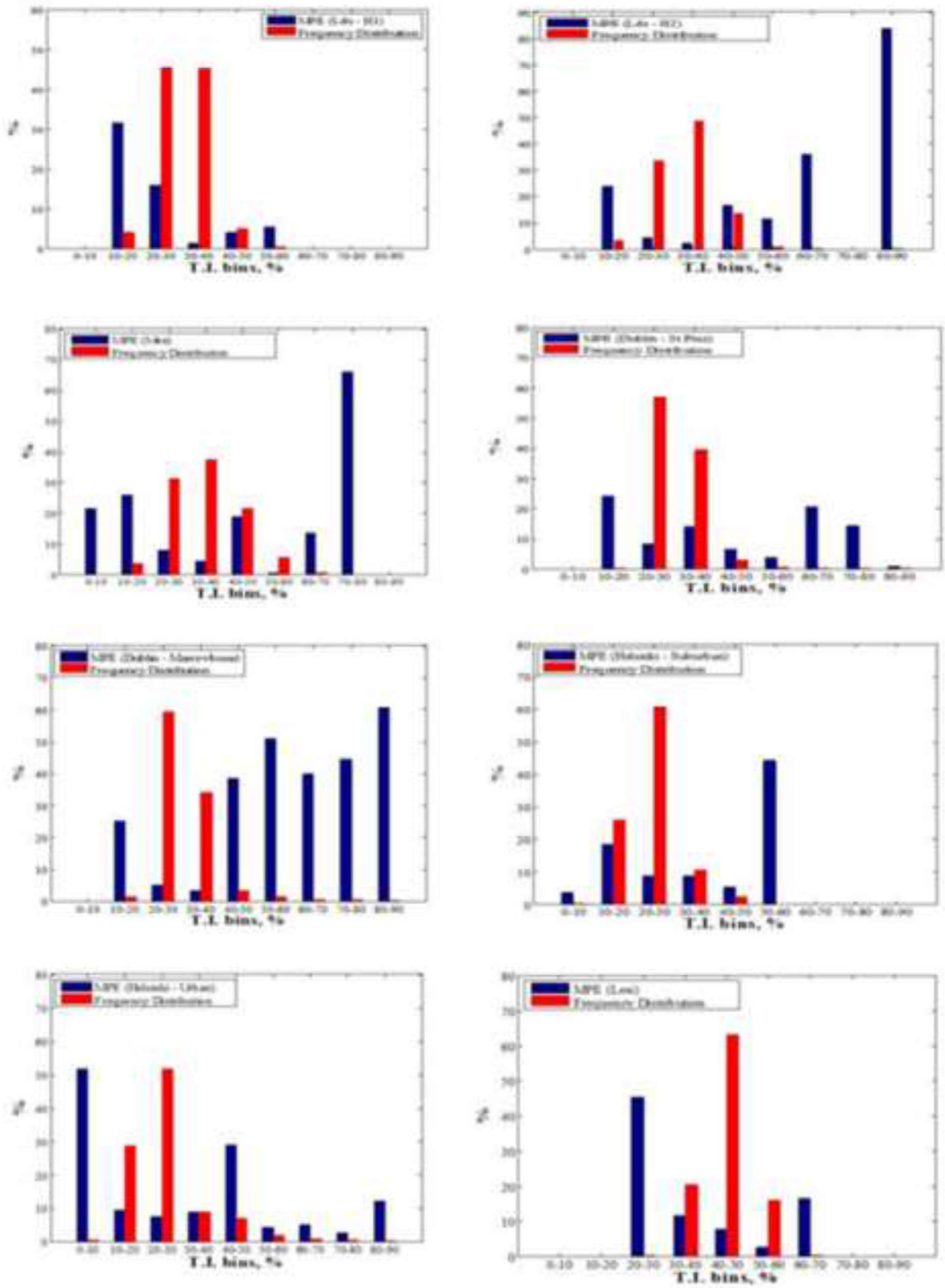

Figure

List of Figures

Figure 12: Overall Average TPE model errors at different response times for all eight potential turbine sites

APPENDIX 1

Figure A. 1: Forces acting on a blade, also demonstrating the chord and the angle of attack relative to the blade as well as the direction of the positive forces described by the direction of the arrows. $\boldsymbol{c}$ represents the blade chord length and β represents the pitch angle (Adapted from [55])

APPENDIX 2

Figure A. 2: Mean Percentage Error (MPE) for turbine power prediction model across all 8 sites at averaging time ($\boldsymbol{T_c}$) of 1 s.

APPENDIX 3

Tables of Lift and Drag coefficients for different Reynolds number at varying angle of attack (alpha) for NACA0012, NACA0015, NACA0018 and NACA0021.

*Declaration of Interest Statement

Declaration of interests

☒ The authors declare that they have no known competing financial interests or personal relationships that could have appeared to influence the work reported in this paper.

☐The authors declare the following financial interests/personal relationships which may be considered as potential competing interests:

***Credit Author Statement**

CREDIT AUTHOR STATEMENT

CRediT roles:

Francis Emejeamara: Conceptualization; Data curation; Formal analysis; Funding acquisition; Investigation; Methodology; Project administration; Resources; Software; Supervision; Validation; Visualization; Roles/Writing - original draft; Writing - review & editing.

Alison Tomlin: Formal analysis; Funding acquisition; Investigation; Methodology; Supervision; Roles/Writing - original draft; Writing - review & editing.